



Importance of plasma discharge characteristics in plasma catalysis: Dry reforming of methane vs. ammonia synthesis

Robin De Meyer^{a,b,c,*}, Yury Gorbanev^a, Radu-George Ciocarlan^d, Pegie Cool^d, Sara Bals^{b,c}, Annemie Bogaerts^a

^a Research group PLASMANT, Department of Chemistry, University of Antwerp, Universiteitsplein 1, 2610 Antwerp, Belgium

^b Research group EMAT, Department of Physics, University of Antwerp, Groenenborgerlaan 171, 2020 Antwerp, Belgium

^c Nanolab Centre of Excellence, University of Antwerp, Groenenborgerlaan 171, 2020 Antwerp, Belgium

^d Research group LADCA, Department of Chemistry, University of Antwerp, Universiteitsplein 1, 2610 Antwerp, Belgium

ARTICLE INFO

Keywords:

Plasma catalysis
Gas conversion
Dry reforming of methane
Ammonia
Microdischarges
Dielectric barrier discharge

ABSTRACT

Plasma catalysis is a rapidly growing field, often employing a packed-bed dielectric barrier discharge plasma reactor. Such dielectric barrier discharges are complex, especially when a packing material (e.g., a catalyst) is introduced in the discharge volume. Catalysts are known to affect the plasma discharge, though the underlying mechanisms influencing the plasma physics are not fully understood. Moreover, the effect of the catalysts on the plasma discharge and its subsequent effect on the overall performance is often overlooked. In this work, we deliberately design and synthesize catalysts to affect the plasma discharge in different ways. These Ni or Co alumina-based catalysts are used in plasma-catalytic dry reforming of methane and ammonia synthesis. Our work shows that introducing a metal to the dielectric packing can affect the plasma discharge, and that the distribution of the metal is crucial in this regard. Further, the altered discharge can greatly influence the overall performance. In an atmospheric pressure dielectric barrier discharge reactor, this apparently more uniform plasma yields a significantly better performance for ammonia synthesis compared to the more conventional filamentary discharge, while it underperforms in dry reforming of methane. This study stresses the importance of analyzing the plasma discharge in plasma catalysis experiments. We hope this work encourages a more critical view on the plasma discharge characteristics when studying various catalysts in a plasma reactor.

1. Introduction

To combat the anthropogenic climate change, many potential solutions are being developed. In the field of plasma-catalytic gas conversion, two main approaches exist. Firstly, greenhouse gases, with a main focus on CO₂, could be converted into environmentally harmless or even useful chemicals. Secondly, existing chemical processes that are responsible for significant greenhouse gas emissions could be electrified in order to produce the required chemicals with renewable energy sources. Examples of such approaches are dry reforming of methane (DRM), where CO₂ and CH₄ are converted into syngas, and NH₃ synthesis, potentially serving as a decentralized alternative to the energy-

intensive Haber-Bosch process [1–5].

Packed-bed dielectric barrier discharge (DBD) plasma reactors are often employed in plasma catalysis, as they allow for an improved contact between the plasma and the catalytic material, since the packed catalyst can be placed inside the discharge volume [6]. The introduction of any packing material will unavoidably change the conditions of the plasma discharge. On the one hand, the packing will decrease the available gas volume, thus decreasing the residence time at a given mass flow rate of the gas, compared to an empty reactor. On the other hand, the packing material will alter the (di)electrical properties of the system, inevitably altering the discharge properties [7]. However, the effect of such packing material on the plasma discharge, and especially its

Abbreviations: BET, Brunauer-Emmett-Teller (analysis); BSE, backscattered electron; DBD, dielectric barrier discharge; DRM, dry reforming of methane; EC, energy cost; EDX, energy dispersive X-ray (spectroscopy); FFT, fast Fourier transform; GC, gas chromatograph; IF, influx fraction; MFC, mass flow controller; MFR, mass flow rate; mln, normal milliliters; NDIR, non-dispersive infrared (spectroscopy); SC, spray-coated; SE, secondary electron; SEL, specific energy input; SEM, scanning electron microscope; SI, supplemental information; WI, wet-impregnated; XRD, X-ray powder diffraction.

* Corresponding author at: Research group PLASMANT, Department of Chemistry, University of Antwerp, Universiteitsplein 1, 2610 Antwerp, Belgium.

E-mail address: robin.demeyer@uantwerpen.be (R. De Meyer).

<https://doi.org/10.1016/j.cej.2024.150838>

Received 14 November 2023; Received in revised form 14 March 2024; Accepted 29 March 2024

Available online 30 March 2024

1385-8947/© 2024 Elsevier B.V. All rights reserved.

subsequent effect on the plasma-catalytic performance, is not yet fully understood. Moreover, when comparing various catalytic materials in plasma catalysis, their effect on the plasma discharge is often overlooked. This makes it difficult to attribute certain changes in e.g. conversion solely to a catalytic effect, when potential differences in the gas phase chemistry are neglected. In plasma catalysis, many physical and chemical processes contribute to the overall performance, which impedes straightforward interpretation and comparison of different studies [8]. Furthermore, optimal (plasma) conditions often differ vastly depending on the reaction of interest. Therefore, we decided to study both DRM and NH_3 synthesis, since they have very different reaction mechanisms and thermodynamic characteristics, the former being endothermic, and the latter being exothermic. Moreover, previous studies indicate that various plasma discharge characteristics could affect the overall performance of these reactions in a different way [9–11].

Often, adequate analysis of the plasma discharge is missing in existing literature reports [12–21], and while indeed sometimes the effect of the catalyst on the plasma discharge was noted in DRM [22–26], NH_3 synthesis [27–35] or for other gas conversion applications [36–39], a systematic investigation of the discharge parameters is rare. Nevertheless, Peeters and van de Sanden proposed a detailed and profound electrical model of a DBD, enabling an extensive study of the discharge parameters based on conventional measurements (i.e., Lissajous figures) and relatively straightforward calculations [40]. Moreover, modeling results indicate that certain aspects of the plasma discharge (e.g. filamentary versus uniform discharge) could indeed affect the gas conversion, independently of any catalytic effect [9–11].

Recently, Brune et al. performed a detailed investigation of the effect of a catalytic packing on the plasma discharge for DRM, with a specific focus on the microdischarges [24]. It was shown that despite identical syntheses using incipient wetness impregnation, different metals had a different effect on the plasma discharge, notably the number of microdischarges. This aberrant behavior was in part attributed to differences in the chemical nature of the catalysts. Likewise, when using a higher metal loading in plasma-catalytic NH_3 synthesis, Ndairinde et al. found that a similar synthesis technique yielded an increased metal concentration at the surface of the support (alumina) beads [35]. The exposed metal was expected to cause drastic alterations of the plasma discharge, which proved to be highly beneficial for NH_3 synthesis. Finally, Seynaeve et al. studied the impregnation of such beads with Fe and Cu and found that small changes in the synthesis protocol could yield significantly different metal distributions [41]. Despite these recent developments, a clear understanding of what causes the changes in the plasma discharge and what precise properties of the plasma affect the overall performance is still lacking.

Therefore, this work focuses on how the catalytic packing material affects the plasma discharge, and how that in turn influences the plasma-catalytic performance. Since metal-loaded (alumina) beads or pellets are often employed in plasma catalysis research, the distribution of the metal on and throughout the beads is emphasized. Two different types of catalysts are designed and synthesized to have drastically different distributions of metal throughout the support beads, deliberately aiming to influence the plasma discharge. These catalysts are synthesized with either Ni or Co as a catalytic metal, supported on porous $\gamma\text{-Al}_2\text{O}_3$ beads. Ni and Co are chosen because they are very often used in plasma-catalytic DRM [42,43] and NH_3 synthesis [35,44,45], respectively. By using metals that are studied frequently, we aim to enable a more straightforward comparison with previous and future work. At the same time, both metals will be used for both reactions in this work, in order to make a direct comparison between the reactions, attempting to understand how the reactions perform under practically identical plasma-catalytic conditions, and to investigate how identical synthesis protocols for different metals can still yield different results. The first type of catalyst is synthesized using the common wet impregnation technique [45], resulting in metal nanoparticles scattered throughout the entire

support bead. The second type of catalyst is synthesized by spray coating [46], a technique which concentrates all deposited metal at the surface of the alumina beads.

These sets of catalysts are used in plasma-catalytic DBD experiments for both DRM and NH_3 synthesis. The performance of the various catalysts is compared with an emphasis on the properties of each plasma discharge. The goal is to elucidate the influence of packed catalysts on the plasma discharge and its subsequent effect on the reaction performance. We explicitly note that the synthesized materials will be called catalysts throughout this work, even though their effect on the reaction may not always be entirely clear, being either physical, chemical, or a combination of both. However, as this is common practice in the plasma catalysis community, this phrasing seems most appropriate.

2. Methods

2.1. Catalyst synthesis

All catalysts were synthesized starting with commercial $\gamma\text{-Al}_2\text{O}_3$ beads (Sasol, product number: 604130) with a diameter of 1.8 mm. Every type of catalyst was synthesized with approximately 30 g of dried beads so that the DRM and NH_3 synthesis experiments could be performed using pristine catalysts from the same batch. Filling the reactor entirely takes around 12.5 g of beads, leaving some margin for losses and analyses.

For the wet impregnation (WI), an aqueous solution of the respective precursor was prepared, $\text{Ni}(\text{NO}_3)_2 \cdot 6\text{H}_2\text{O}$ (Sigma-Aldrich, 97.5 %) for the Ni catalyst and $\text{Co}(\text{NO}_3)_2 \cdot 6\text{H}_2\text{O}$ (Sigma-Aldrich, >98 %) for the Co catalyst. The amount of precursor was chosen to yield a final metal loading of 10 wt% and the volume of the solution was chosen to correspond to 0.75 ml per g of Al_2O_3 beads, as that was empirically determined to be the volume of liquid the beads can absorb. After drying the beads, the precursor solution was added to the beads, followed by continuous stirring for a few minutes to ensure a homogeneous distribution of the precursor. Next, the beads were left to dry in ambient conditions overnight after which they were dried at 120 °C for 24 h. Further, the beads were calcined in air at 400 °C for 6 h and finally reduced in a tube furnace with 2 % H_2 in Ar (Air Liquide, >99.999 %) for 8 h at 550 °C. Note that this reduction step was only done overnight immediately prior to plasma-catalytic experiments, to limit the potential re-oxidation of the catalysts through prolonged storage.

The spray-coated (SC) catalysts were prepared according to a protocol adapted from Uytendhouwen et al. [46]. In preliminary synthetic experiments, the 10 wt% catalysts proved to be too structurally unstable for further use in the plasma catalysis experiments, because the much thicker shell obtained with this high amount of metal partially detached from the beads, making the estimate of the loading highly inaccurate. Therefore, only 3.3 wt% and 1 wt% Ni and Co catalysts will be discussed from here onwards. An aqueous solution of the respective precursors was prepared ($\text{Ni}(\text{NO}_3)_2 \cdot 6\text{H}_2\text{O}$ and $\text{Co}(\text{NO}_3)_2 \cdot 6\text{H}_2\text{O}$) with a concentration of approximately 0.6 M in amounts to yield the correct metal loading of either 3.3 or 1 wt%. This solution was stirred and heated to 80 °C. Next, a 3 M NaOH (Acros Organics, 98.5 %) solution of approximately the same volume as the Ni/Co solution was added to the precursor while stirring continuously. This volume ensured a very basic environment, promoting the precipitation of the Ni/Co species. When adding the NaOH solution, a Ni or Co oxyhydroxide was formed and precipitated. After stirring for 2 h at 80 °C, the precipitate was left to settle under static conditions. Next, the clear supernatant was removed and 150 ml of water was added followed by stirring for a short time. The precipitate was again left to settle and this washing step was done three times in total. After the washing steps with water, the same washing steps were done three times using isopropanol (Merck, >99.8 %). This procedure finally yielded a suspension of either Ni or Co oxyhydroxides in isopropanol. For the actual spray coating, the dried Al_2O_3 beads were placed in a rotating drum, after which the prepared suspension was

slowly sprayed on the rotating beads. Warm air was sent into the drum to promote rapid evaporation of the solvent, while the spraying was done intermittently to prevent the suspension from entering the pores. Finally, after all the suspension was sprayed and most of the solvent evaporated, the beads were left to dry overnight in ambient conditions. Identical to the wet impregnated catalysts, these beads were then dried for 24 h at 120 °C, calcined in air at 400 °C for 6 h and reduced in 2 % H₂ in Ar at 550 °C for 8 h.

2.2. Catalyst characterization

2.2.1. Scanning electron microscopy

To investigate the metal distribution throughout the beads as well as the metal coverage at the surface of the beads, and the total metal loading of the WI catalysts, scanning electron microscopy (SEM) and energy dispersive X-ray spectroscopy (EDX) analyses were performed using a Thermo Fisher Scientific Quanta 250 ESEM equipped with an Oxford Instruments EDX detector. Prior to SEM analysis, two beads of every batch were embedded in an epoxy resin (EPO-TEK 353ND-T4), ground and polished to expose a smoothed cross-section of each bead. These samples were then attached to an SEM-stub and coated with a circa 10 nm layer of C to improve the conductivity during SEM analysis. EDX maps were acquired from the cross section and quantified to yield a radial distribution of the catalyst metal throughout the bead [35], as described in more detail in the Supplemental Information (SI, Section S1, Fig. S1). Furthermore, whole beads were glued to an SEM-stub using silver paint and coated with a circa 10 nm layer of C to investigate their surface. Samples were analyzed using either secondary electron (SE) or backscattered electron (BSE) imaging [47]. SE-SEM imaging is very sensitive to surface topography, which was employed here to study the structure of the SC shell at the surface of the beads. BSE-SEM imaging is sensitive to the atomic mass of the sample and was therefore used to study the distribution and coverage of Ni or Co at the surface of the beads, yielding a higher signal compared to the lighter Al₂O₃ background.

2.2.2. X-ray powder diffraction

To determine the oxidation state of the metal loaded on the catalyst, X-ray powder diffraction (XRD) was used to characterize the various samples. For these analyses, a Bruker D8 ADVANCE eco XRD machine

was used, operating with a Cu K- α X-ray source. The beads were crushed in a mortar prior to XRD analysis.

2.2.3. N₂ sorption

In order to probe the specific surface area of the various catalysts, N₂ sorption at 77 K and subsequent Brunauer-Emmett-Teller (BET) analysis was performed. The sorption measurements were performed using a Quantachrome Quadrasorb SI analyzer and the BET calculations were carried out using QuadraWin software.

2.3. Plasma reactor setup

A schematic representation of the setup is provided in Fig. 1, whereas the exact dimensions of the reactor are presented in the SI (Section S2, Fig. S3). The reactor consists of a ceramic tube (alumina, Ceratec) wrapped with a 100 mm wide metal mesh that acts as the powered electrode. A steel rod placed through the ceramic tube acts as the grounded electrode and creates a gap of 4.5 mm between the rod and the ceramic tube that is packed with the (catalyst) beads. The catalysts were held in place by glass wool at both ends and the gases were sent to the reactor through mass flow controllers (Bronkhorst). A 23.5 kHz sinusoidal voltage was applied by the G10 S-V (AFS GmbH) power supply unit (PSU) and sent to the outer electrode of the reactor through a transformer with a constant applied PSU power of 100 W. A high voltage probe (Tektronix P6015A) was used to measure the applied voltage via the digital oscilloscope (Pico Technology PicoScope 6402A). The central rod was connected to the ground through a capacitor (10 nF) over which the voltage was monitored by the oscilloscope through a voltage probe (Pico Technology TA150). The current through the grounded cable to the capacitor was measured using a current monitor (Pearson Electronics 4100), also connected to the oscilloscope.

For the DRM experiments, a mixture of CO₂ and CH₄ (Air Liquide, >99.998 % and > 99.995 %, respectively) was sent to the reactor at a total flow rate of 100 ml/min (normal ml per min) [48] in a CO₂/CH₄ ratio of 1:1 or 2:1. We emphasize that we controlled the mass flow rate (and not volumetric flow rate) in the experiments, which was measured in ml/min. The outflow of the reactor was sent through a cold trap to condense the liquid fraction, which was determined to be mostly water (>98 %) with small amounts of methanol and ethanol by a separate gas chromatography (GC) measurement. Further, the total volume of the

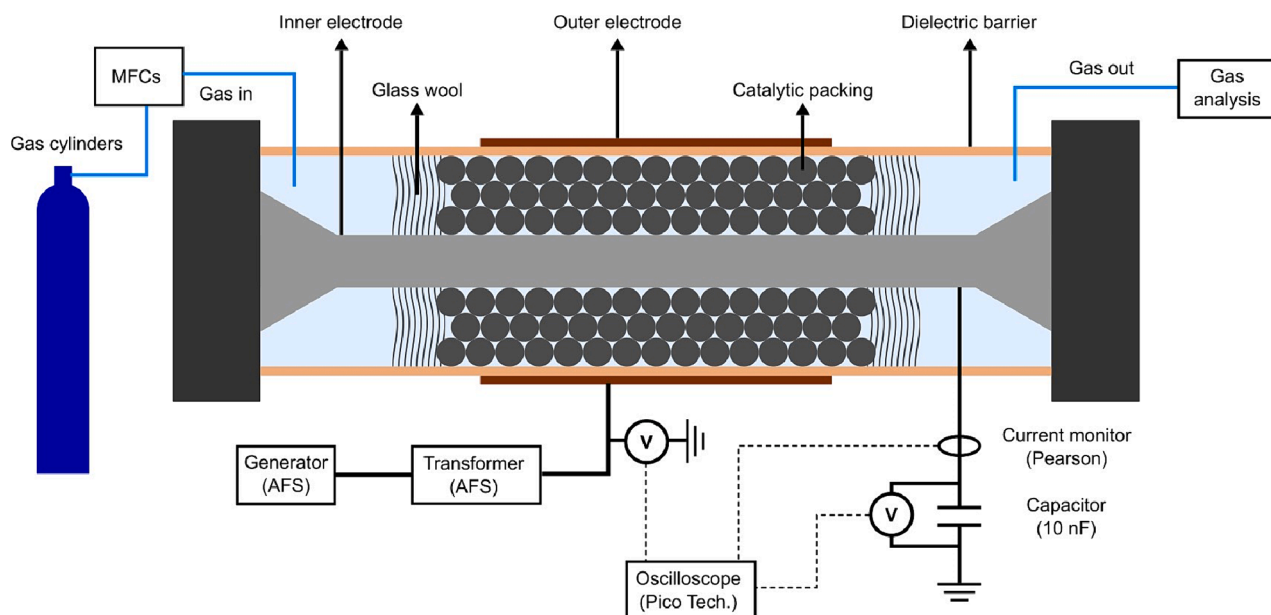


Fig. 1. Schematic representation of the reactor setup. The “Gas analysis” consists of an NDIR for NH₃ synthesis, or of a cold trap followed by a GC for the DRM experiments.

liquid fraction was very small (in the order of a few hundred μl), which prevented an accurate measurement. After the cold trap, the online GC (Agilent 990 Micro GC) sampled gas from the exhaust line to determine its composition. The GC was equipped and calibrated to measure CO_2 , CH_4 , CO , O_2 , H_2 , N_2 , C_2H_2 , C_2H_4 , and C_2H_6 . As gas expansion can influence the measurements [49,50], N_2 was used as a standard for the GC measurements, by adding a continuous flow of 20 mln/min N_2 to the outflow of the reactor before sampling by the GC. Before every experiment, the GC sampled at least three times to determine a baseline for the concentrations of the gases entering the reactor and used as a standard. The plasma was on for 1 h for each experiment with the GC sampling approximately every 5 min. This allowed the system to reach quasi-steady state after around 15 min, which then left enough samples to average the measurements. These peaks in the chromatograms were integrated, averaged over the samples during the quasi-steady state and converted to concentrations using our calibration. The standard deviation of the various peak areas and the error on the calibration were used to determine the error on the concentration of every component.

For the NH_3 synthesis experiments, a mixture of N_2 and H_2 (Air Liquide, >99.999 %) with a total flow rate of 100 mln/min was sent to the reactor. For these experiments, N_2/H_2 ratios of 3:1, 1:1 and 1:3 were used. The outflow of the reactor was then analyzed by a non-dispersive infrared sensor (NDIR, Rosemount X-stream Enhanced XEGP Continuous Gas Analyzer, Emerson). The plasma was on until the NH_3 concentration in the outflow remained stable for at least 10 min, which was then averaged over this stable area to determine an overall NH_3 concentration for that experiment. An illustration of the evolution of the NH_3 concentration as a function of time is provided in the SI (Section S3, Fig. S4). The standard deviation of the set of stabilized concentration measurements was used as the error on the measurements.

To mimic the residence time of a packed reactor, experiments for all gas mixtures were also performed with an empty reactor at 200 mln/min, as the packing is expected to occupy roughly half of the volume of the reactor, thus approximately reducing the apparent residence time by a factor of two [51].

2.4. Discharge characterization

During the plasma experiments, various snapshots were acquired by the oscilloscope, monitoring the applied voltage and the measured current. During operation, the charge–voltage (Q-V) diagram, so-called Lissajous figure, was also shown to monitor the discharge during the experiment. For the detailed analysis of the discharges, only the applied voltage and the measured current were used. This method was compared in the SI (Section S4) to another common technique of using the voltage over the monitoring capacitor, which proved to be practically identical. Many of the analyses characterizing the discharge are based on the work of Peeters et al. [40,52].

During each experiment, multiple (at least three) snapshots were acquired with the oscilloscope when a (quasi-)steady state was reached, saving the applied voltage and measured current. The electrical measurements coincided with the gas-phase analyses, thus not including the initial phase of the experiment. Each of these snapshots was analyzed to yield the various discharge characterizing metrics (i.e., plasma power, microdischarge quantity, effective dielectric and cell capacitances, burning voltage, conductively transferred charge, as discussed in detail below) and the variation between the snapshots was used to determine an error on the various characteristics.

The first important property of the DBD plasma, is the plasma power P . This is determined by multiplying the applied voltage V and the measured current I and taking the average of these values over a whole number of cycles (11 in one snapshot in our case). This is illustrated in Eq. (1).

$$\bar{P} = \frac{1}{T} \int_0^T V(t) \bullet I(t) dt \quad (1)$$

Further analyses of the plasma discharge are based on the work of Peeters and van de Sanden [40], accounting for partial surface discharging. Note that this electrical model we employ was developed for a system without a packing material. Hence, caution is advised when applying these equations to our data. However, there is no model in literature for a packed bed DBD, and we believe this approach is justified, because the packing can be seen as a part of the gap, indeed drastically changing its properties (as described below), but not necessarily breaking the proposed model.

In order to do these analyses, the geometric dielectric capacitance C_{diel} has to be determined. This capacitance is inherent to the reactor setup, but it is challenging to measure. Therefore, a theoretical calculation is used to approximate this capacitance, as shown in Eq. (2)

$$C_{diel} = \frac{2\pi k \epsilon_0 L}{\ln \frac{b}{a}} \quad (2)$$

with k the dielectric constant of the material used for the dielectric barrier (10, as provided by the manufacturer), ϵ_0 the permittivity of vacuum, L the length of the discharging part of the reactor (100 mm), b the outer diameter of the dielectric cylinder (22 mm) and a the inner diameter of the cylinder (17 mm). This yields a dielectric capacitance of 216 pF, which is needed for the further calculations. As Eq. (2) is based on an ideal system and the dielectric constant is not known with great precision, a relative error of 10 % on the dielectric capacitance will be used in further error propagation calculations.

Next, the effective dielectric capacitance ζ_{diel} and the cell capacitance C_{cell} can be extracted directly from the Lissajous figures by fitting a straight line to the beginning (“plasma-off” segment) and end (“plasma-on” segment) of the rising side of the curve for C_{cell} and ζ_{diel} , respectively (illustrated in Fig. 2). These calculations were performed for every full PSU cycle in the oscilloscope snapshots. The obtained values were found to be effectively identical to those extracted from averaged Lissajous figures, as presented in the SI (Section S5).

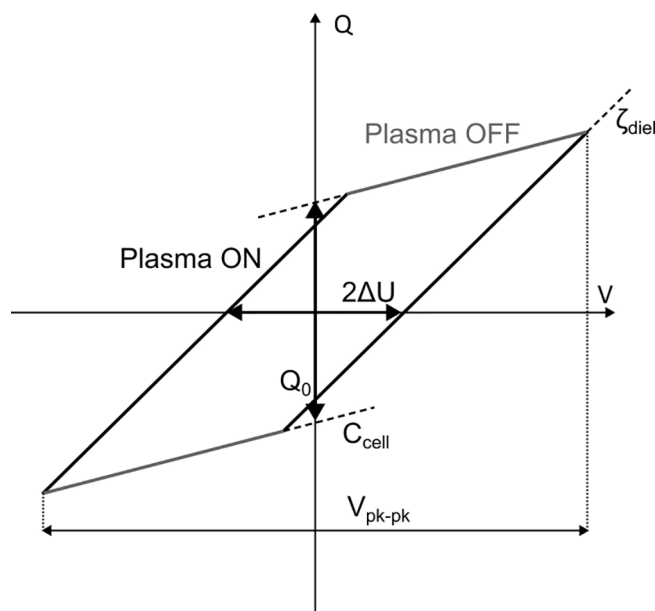


Fig. 2. Illustration of parameters extracted from the Lissajous figures. The derivative of the “plasma off” section yields the cell capacitance C_{cell} , the derivative of the “plasma on” section yields the effective dielectric capacitance ζ_{diel} , the difference between the maximum and the minimum of the applied voltage yield the peak-to-peak voltage V_{pk-pk} , the difference between the voltages at which the charge crosses zero yields $2\Delta U$, which is used to calculate the burning voltage U_b , and the difference in charge between the (ideally parallel) “plasma off” sections yields Q_0 , which is used to calculate the conductively transferred charge ΔQ_{dis} .

Further, the partial discharging can be quantified. Partial surface discharging is the effect where the plasma is only formed in a part of the reactor, thus neglecting certain areas of the dielectric barrier, the so-called non-discharging areal fraction α [40]. This is a defining characteristic of the DBD plasma discharge and, among other things, causes a discrepancy between the true and measured (or effective) dielectric capacitances (C_{diel} and ζ_{diel} , respectively). Eq. (3) describes how α can be calculated based on the measured and estimated dielectric capacitances and cell capacitance, discussed earlier.

$$\alpha = \frac{C_{diel} - \zeta_{diel}}{C_{diel} - C_{cell}} \quad (3)$$

Analogously, the discharging areal fraction β can be defined as:

$$\beta = 1 - \alpha \quad (4)$$

In an ideal, fully discharging (i.e. $\alpha = 0$) DBD, the burning voltage is measured as half of the distance between the zeros ($Q = 0$) of the Lissajous figures (see again Fig. 2). When accounting for partial discharging, this measured burning voltage ΔU can be converted to a true burning voltage U_b :

$$U_b = \pm \left(1 + \frac{\alpha C_{cell}}{\beta C_{diel}} \right) \Delta U = \frac{1 - \frac{C_{cell}}{C_{diel}}}{1 - \frac{C_{cell}}{\zeta_{diel}}} \Delta U \quad (5)$$

Next, the conductively transferred charge ΔQ_{dis} can be calculated based on the measured charge difference between the two “plasma-off” phases Q_0 . This Q_0 can be extracted from the measured Lissajous figures by determining the difference between the intersects of the fitted “plasma-off” curves with the Q-axis (see again Fig. 2). Then, ΔQ_{dis} can be calculated using the following equation:

$$\Delta Q_{dis} = \frac{Q_0}{1 - \frac{C_{cell}}{C_{diel}}} \quad (6)$$

Additional details and theoretical background regarding these equations can be found in the work of Peeters and van de Sanden [40].

Another important, though hard to quantify, discharge characteristic in a DBD is the number and intensity of microdischarges. These short-lived, localized and intense discharges are typical in many DBD experiments and they have a significant impact on the gas-phase chemistry [9–11], yet they are tricky to quantify [53]. Firstly, the hardware requirements to precisely measure the fast change in current are stringent. Further, the interpretation of the data is rarely straightforward. For example, it is challenging for an automated analysis to accurately “count” the number of microdischarges when multiple discharges are taking place at the same time in the reactor. Alternatively, manual counting is rarely desirable as it is labor-intensive and sensitive to human error and bias. As the current monitor used in this work (Rogowski coil, Pearson Electronics 4100, with a rise time of 10 ns [54]) struggles to capture the true structure of microdischarges, we did not attempt to “count” the number of microdischarges, let alone try to integrate them individually, as this would have introduced too many uncertainties. Rather, we took a more general and prudent approach by defining a “microdischarge quantity”, based on the frequency spectrum of the current signal. As our hardware is at its limit to measure the microdischarges, but not entirely incapable, we assume that microdischarges are still registered, albeit slightly deformed. First, we calculated the capacitive displacement current $I_{displacement}$ and subtracted it from the measured current I to yield the true plasma current I_{plasma} . The displacement current $I_{displacement}$ is calculated using the following equation (see SI Section S6 for more details) [40,52]:

$$I_{displacement}(t) = C_{cell} \frac{dV(t)}{dt} \quad (7)$$

Next, we applied the fast Fourier transform (FFT) to the plasma current

signal, and integrated over a wide frequency range from 10 to 100 MHz, corresponding to a time-scale range of 10 to 100 ns. This value does not have an immediate physical interpretation, but it allows for an objective, relative comparison between experiments with various catalysts. For example, both a larger number of microdischarges, and a higher current spike during the microdischarges, will increase the “microdischarge quantity”, so it can be seen as a combination of the number and intensity of the microdischarges. More details on this quantification can be found in the SI (Section S7).

2.5. Performance metrics

2.5.1. Dry reforming of methane

The DRM reaction proceeds as follows:



Hence, the formation of additional gas molecules (see reaction (R1)) causes an expansion of the gas. On the other hand, solid carbon deposition, formation of larger molecules, and condensation of liquid components could cause a contraction of the gas mixture. Therefore, the flux ratio α_{flux} was determined empirically with the standard method (i.e., by adding a fixed flow of the standard N_2 and monitoring its concentration), using the following equation [49,50]:

$$\alpha_{flux} = \frac{y_{in}^{IS}}{y_{out}^{IS}} \quad (8)$$

with y_{in}^{IS} the fraction of “internal standard” (N_2) without plasma and y_{out}^{IS} the fraction of N_2 with plasma, as measured by the GC.

Next, the absolute conversion X^{abs} of CO_2 and CH_4 can be calculated. The absolute conversion only considers the individual reactant and how much of the used reactant was actually converted:

$$X_i^{abs} = \frac{y_i^{in} - \alpha_{flux} y_i^{out}}{y_i^{in}} \quad (9)$$

with i the reactant of interest (either CO_2 or CH_4), y_i^{in} the fraction of reactant i as measured without plasma and y_i^{out} the fraction of reactant i as measured with plasma. The total conversion X^{tot} can then be determined by combining both absolute conversions, weighted by their respective fraction in the influx. The influx fractions IF are calculated based on the measured concentration of CO_2 and CH_4 without plasma:

$$IF_i = \frac{y_i^{in}}{y_{CO_2}^{in} + y_{CH_4}^{in}} \quad (10)$$

Combined with these influx fractions, the absolute conversions can be used to calculate the total conversion:

$$X_{tot} = X_{CO_2}^{abs} * IF_{CO_2} + X_{CH_4}^{abs} * IF_{CH_4} \quad (11)$$

Taking into account the measured plasma power P , the specific energy input (SEI) can be calculated:

$$SEI = \frac{P}{Q_{in}} \quad (12)$$

with Q_{in} the flow rate going into the reactor. Next, the energy cost (EC) can be determined by combining the SEI with the total conversion:

$$EC_{DRM} = \frac{SEI}{X_{tot}} \quad (13)$$

This EC_{DRM} has the same unit as the SEI , and they can be expressed in different units (e.g. kJ/l or kJ/mol), depending on conversion factors in the formulas [50]. It should be interpreted as the amount of energy used for the conversion of CO_2 and CH_4 .

Further, the selectivity towards certain products j based on atoms A

can be determined:

$$S_j^A = \frac{\mu_j^A \alpha_{flux,j}^{out}}{\sum_i \mu_i^A (y_i^{in} - \alpha_{flux,i}^{out})} \quad (14)$$

with μ_j^A the number of atoms A in product j and μ_i^A the number of atoms A in reactant i .

2.5.2. NH_3 synthesis

During the NH_3 synthesis experiments, the outflow of the reactor was analyzed by an NDIR, measuring the NH_3 concentration in the gas mixture. As only one chemical reaction takes place, the stoichiometry of that reaction suffices to take the gas contraction into account (see Reaction (R2)).



Knowing this, the mass flow rate of NH_3 in the outflow of the reactor ($MFR_{NH_3}^{out}$) can be calculated:

$$MFR_{NH_3}^{out} = \frac{MFR_{tot}^{in} y_{NH_3}^{out}}{1 + y_{NH_3}^{out}} \quad (15)$$

where MFR_{tot}^{in} is the combined flow rate of N_2 and H_2 at the inlet and $y_{NH_3}^{out}$ is the measured fraction of NH_3 at the outlet. Similar to DRM, an energy cost (EC_{NH_3}) can be defined for the NH_3 synthesis. However, this EC_{NH_3} is defined slightly differently, namely as the amount of energy used for

the production of the synthesized NH_3 , rather than for the conversion of reactants, as in the case of DRM:

$$EC_{NH_3} = \frac{P}{MFR_{NH_3}^{out}} \quad (16)$$

3. Results and discussion

3.1. Catalyst synthesis and characterization

For the WI catalysts, SEM-EDX maps were acquired from cross sections of the beads. The acquired data was processed as described in the SI (Section S1) to yield a radial distribution of the catalyst metal throughout the alumina beads, as well as a total metal loading. The distributions, shown in Fig. 3A, illustrate that the catalyst metals are distributed homogeneously throughout the entire bead, penetrating to the center of the beads, with a slight increase in concentration towards the edge. The total metal loadings (11.1 wt% and 10.0 wt% for the Ni and Co beads presented in Fig. 3A, respectively) agree with the expected 10 wt%. Measurements of a second bead of each catalyst are presented in the SI (Section S1, Fig. S2) and are in good agreement with the first measurements.

Notably, the BSE-SEM images of the surfaces of the WI catalysts show a discrepancy in metal nanoparticle coverage between the Ni and Co catalyst, as illustrated in Fig. 3B and C. The BSE signal is higher at the position of heavier atoms, thus highlighting the Ni and Co nanoparticles

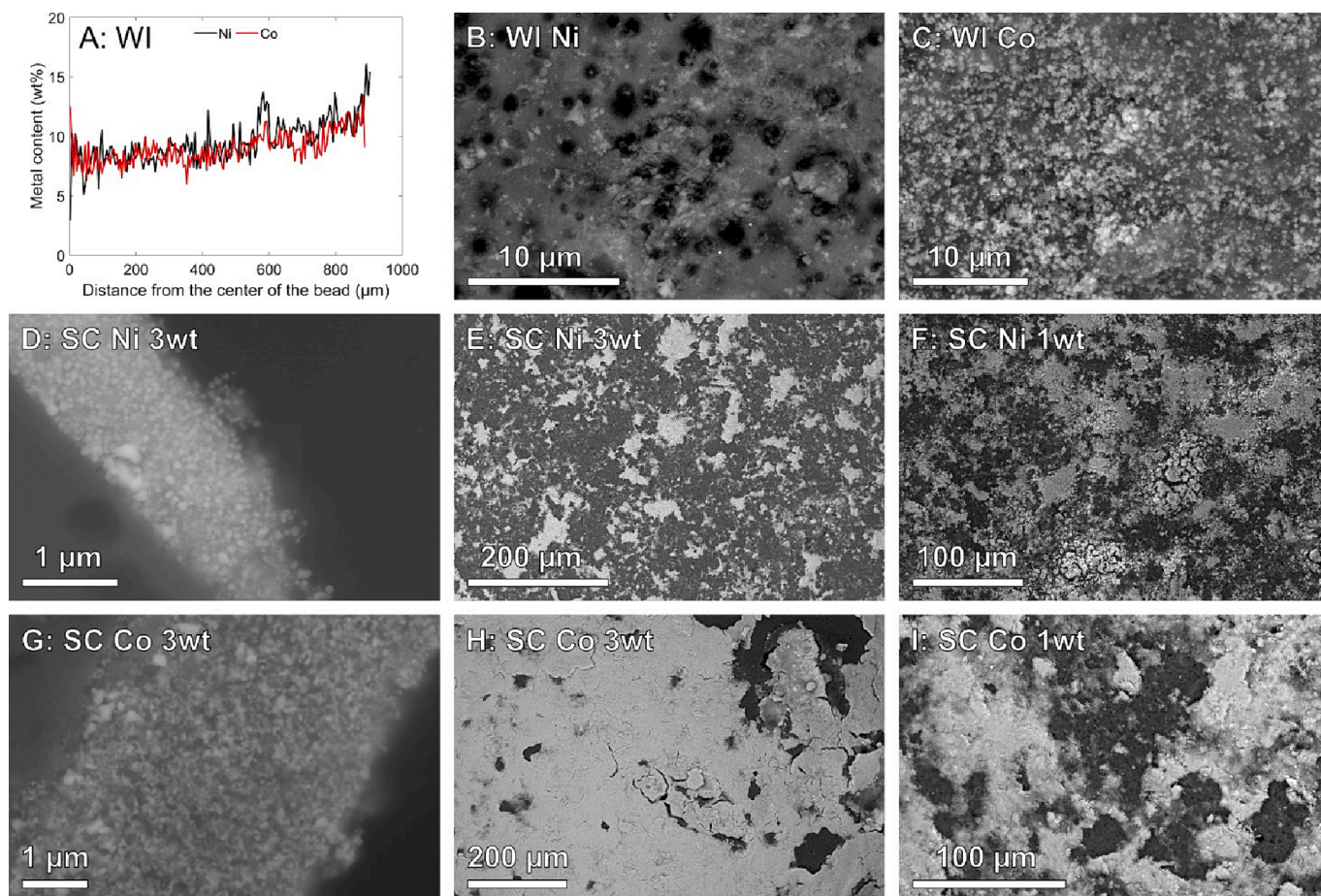


Fig. 3. SEM analyses of the various catalysts. A: Radial distribution of Ni and Co throughout WI beads; total metal loadings for these catalysts are 11.1 wt% (Ni) and 10.0 wt% (Co). B: BSE-SEM image of the surface of a WI Ni bead. C: BSE-SEM image of the surface of a WI Co bead. D: SE-SEM image of a cross-section of a SC Ni 3 wt% bead, presenting the nanoparticles inside the Ni shell at the surface of the bead. E: BSE-SEM image of the surface of a SC Ni 3.3 wt% bead. F: BSE-SEM image of the surface of a SC Ni 1 wt% bead. G: SE-SEM image of a cross-section of a SC Co 3.3 wt% bead, presenting the nanoparticles inside the Co shell at the surface of the bead. H: BSE-SEM image of the surface of a SC Co 3.3 wt% bead. I: BSE-SEM image of the surface of a SC Co 1 wt% bead.

against the Al_2O_3 background. It is clear that the WI Co catalyst have a substantially higher coverage of nanoparticles at the surface compared to the WI Ni catalyst. A similar accumulation of Co particles at the surface of the catalyst was observed by Ndayirinde et al. for their Co-based WI catalysts [35]. The accumulation they observed was even more pronounced, though they used an adapted synthesis method and used a much higher metal loading. More advanced synthesis protocols may be employed to obtain more control over the precise metal distribution [55,56].

The SEM analyses of the SC beads reveal a clear shell at the surface of the beads. The shell consists of metal(oxide) nanoparticles, as evidenced in Fig. 3 D (Ni) and G (Co). Moreover, the BSE-SEM images of the surface of the beads in Fig. 3E, F, H, and I reveal that the shell is relatively inhomogeneous for Ni, while for Co the layer at the surface is mostly homogeneous, with some sections missing. It is likely that by manipulating the beads, some parts of the shell detached, as a strong interaction between the particles in the shell is lacking. For the SC Ni catalysts, the thickness of the shell varies between hundreds of nm to a few μm . For the SC Co beads, the shell thickness also varies, but it is much more consistent. In this case, it is also obvious that for the 3.3 wt% beads, the shell is clearly thicker (approximately $5\ \mu\text{m}$) than for the 1 wt% beads ($0.5\text{--}2\ \mu\text{m}$). Additional SEM images of the cross-sections of the SC catalysts are provided in the SI (Section S8, Fig. S15).

The XRD measurements show that the reduction of the SC catalysts was completed, as no reflections corresponding to either Ni- or Co-oxides remained (see SI Section S8, Figs. S16 and S17). For the WI

catalysts, however, both Ni and Co metal and oxides phases are present. This is likely due to the inaccessibility of the innermost Ni- or Co-oxide particles during the reduction step, likely because H_2 cannot penetrate deep enough into the pores during the reduction.

The N_2 sorption results indicate that the specific surface area decreases slightly after deposition of the catalysts compared to the blank alumina beads (see SI, Section S10). The decrease of the specific surface area is the highest for the WI catalysts ($180\text{--}190\ \text{m}^2/\text{g}$) and is least pronounced for the 1 wt% SC catalysts (approximately $220\ \text{m}^2/\text{g}$), with a specific surface area of blank alumina of approximately $240\ \text{m}^2/\text{g}$. We attribute the observed effects for the WI catalysts to the penetration of the loaded metal/metal oxides deep inside the beads during WI, effectively blocking or filling the pores throughout the whole bead rather than just the surface, causing the more significant decrease in specific surface area. This further elucidates the partial oxidation of the WI catalysts, since the blocked pores are then inaccessible for the H_2 during the reduction step. The SC particles, however, remain at the surface, preserving the porosity inside the beads. Further, the SC layer of Ni or Co is patchy and consists of particles (see Fig. 3), rather than a bulk layer, thus allowing most of the N_2 to penetrate inside the pores.

3.2. Effect of the catalysts on the plasma discharge

The two main measurements of the plasma discharge and its properties are the current–voltage (I–V) characteristics and the Lissajous (charge–voltage; Q–V) figures. These measurements offer insights in the

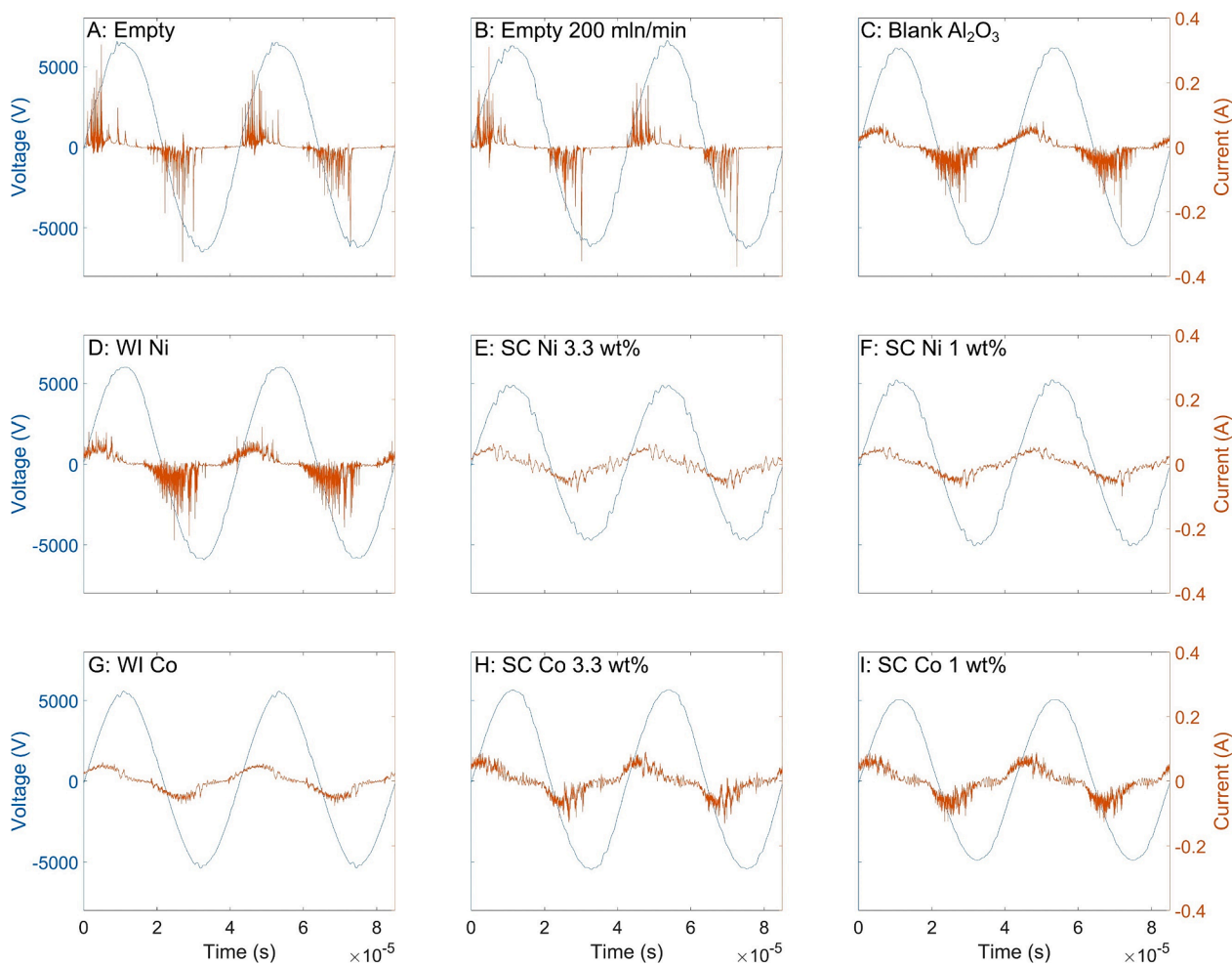


Fig. 4. Representative I–V curves of the calculated plasma current I_{plasma} for all experimental sets of DRM for a CO_2/CH_4 ratio of 1:1, illustrating the clear filamentary regime for the empty reactor, the reactor with blank Al_2O_3 packing and with WI Ni catalyst, while these filaments virtually disappear for the WI Co and the various SC catalysts.

plasma discharge, enabling a direct comparison between the various experiments using different catalysts. Representative I-V characteristics displaying the calculated plasma current I_{plasma} and Lissajous figures of the DRM experiments and NH_3 synthesis experiments are provided in Fig. 4 (I-V, DRM), Fig. 5 (I-V, NH_3), Fig. 6 (Lissajous, DRM), and Fig. 7 (Lissajous, NH_3). The measured current and the capacitive displacement current are shown in the SI (Figs. S9–S12). While the overall shape of the current trace is affected in some cases by the subtraction of the capacitive displacement current, the high-frequency characteristics of the various signals (i.e., the microdischarges) are preserved.

For the empty reactor, as well as when it is packed with blank Al_2O_3 beads or with the WI Ni/ Al_2O_3 catalysts, plenty of microdischarges are observed in the current signal, manifesting as short but intense bursts of current, illustrated in Fig. 4(A–D) for DRM and Fig. 5(A–D) for NH_3 synthesis. These microdischarges are strongly affected when introducing SC catalysts or the WI Co catalyst (see Fig. 4(E–I) for DRM and Fig. 5 (E–I) for NH_3 synthesis). Note that the behavior of the SC Ni 1 wt% is aberrant in the case of NH_3 synthesis (Fig. 5F), most likely due to the instability of the catalyst, where the shell detached significantly during the manipulation of the beads (see Fig. 3).

This drastic alteration of the discharge behavior is attributed to the presence of metallic nanoparticles at the surface of the beads (thus exposed to the plasma). The discrepancy in the behavior between WI Ni and WI Co further supports this hypothesis, as the WI Co had

significantly more Co particles at the surface compared to Ni particles on the WI Ni beads (see the SEM analysis, Fig. 3B and C). We hypothesize that the exposed metal throughout the reactor volume “seeds” the plasma with electrons, so that the discharge can be initiated and sustained uniformly throughout the reactor volume. Alternatively, the discharge may consist of many, very weak “microdischarges”, yielding this seemingly more uniform discharge, rather than the more common highly filamentary discharge mode [57]. The underlying mechanism that provides these electrons is not fully understood and may be a combination of various effects, such as secondary electron emission [58] (potentially due to enhanced surface roughness [59]), surface Penning ionization (also known as Auger de-excitation) [60,61], field emission [62], or others. Further, the metal present at the surface is also expected to significantly affect the formation and propagation of surface ionization waves, which typically play an important role in packed-bed DBD plasma reactors [63,64].

Note that these effects can be very sensitive to physical and chemical differences, such as particle size and surface oxidation, which implies that minor changes in the catalyst properties can affect the plasma discharge, which in turn can alter the chemistry of the gas phase. However, these hypotheses remain somewhat speculative, since the precise mechanisms that enable a diffuse discharge in a DBD are not yet fully understood (not in the least for packed-bed systems) [65]. Recently, Bajon et al. were able to achieve a diffuse CO_2 plasma in a non-

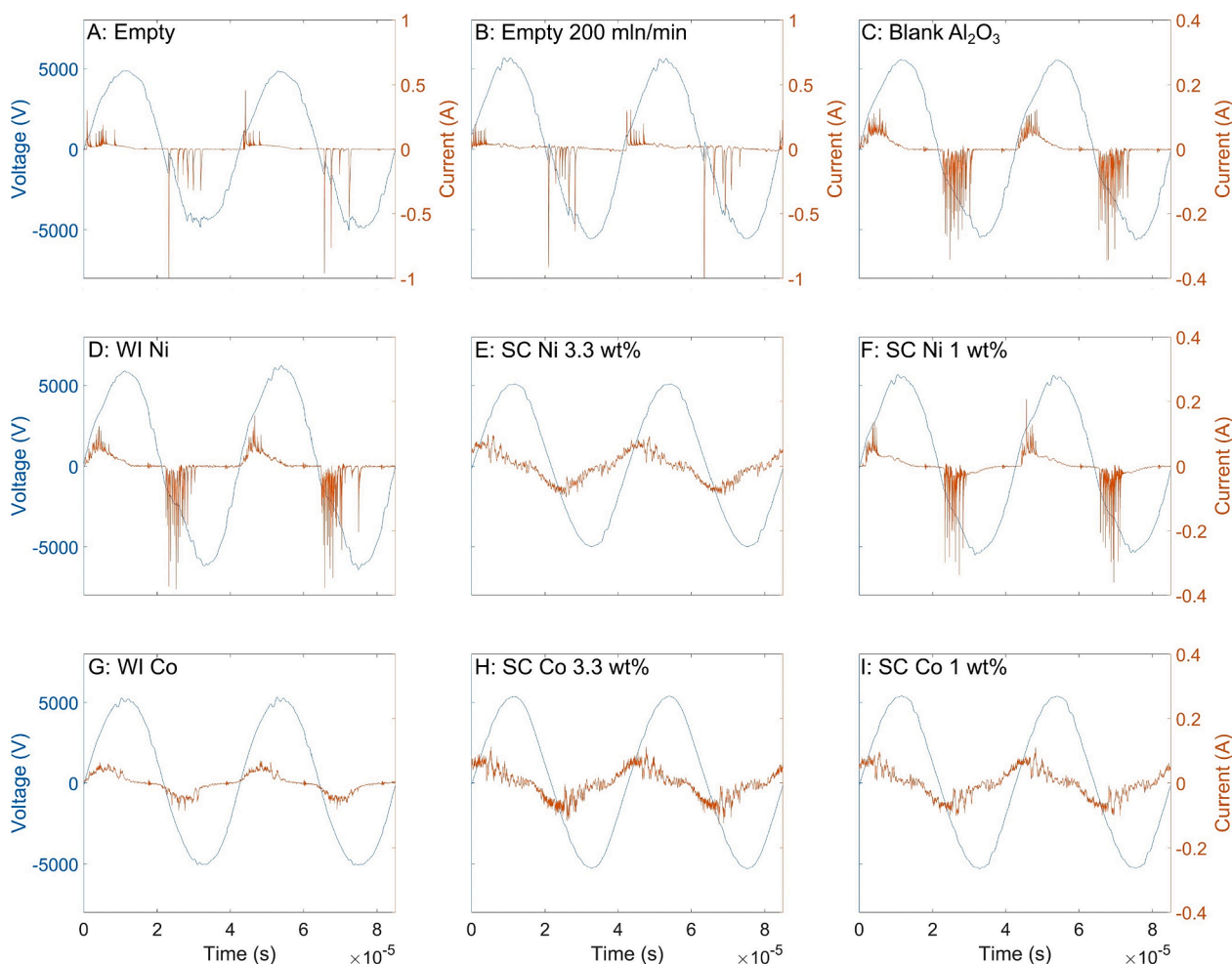


Fig. 5. Representative I-V curves of the calculated plasma current I_{plasma} for all experimental sets of NH_3 synthesis for a N_2/H_2 ratio of 1:1. Note that the y-axes of the current are wider for the empty reactor at both 100 and 200 ml/min (A,B) compared to the other graphs to prevent clipping the signal while still giving a clear representation of the signal for the other graphs. This figure again illustrates the clear filamentary regime for the empty reactor, the reactor with blank Al_2O_3 packing and with WI Ni catalyst, while these filaments virtually disappear for the WI Co and the various SC catalysts (with the exception of SC Ni 1 wt%, probably due to instability of the catalyst; see text).

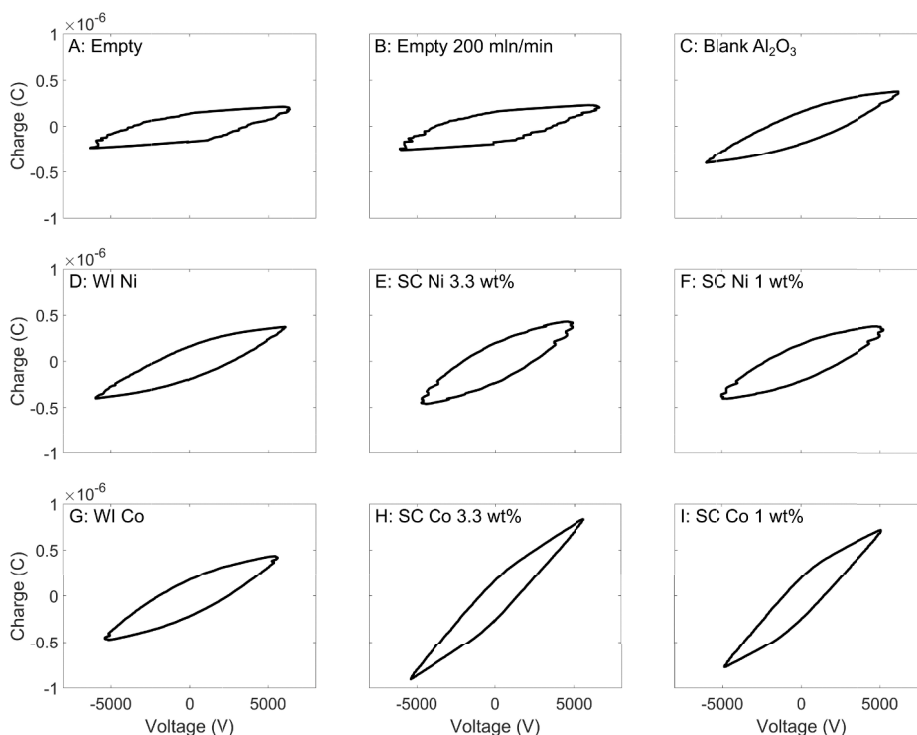


Fig. 6. Representative Lissajous figures for all experimental sets of DRM for a CO_2/CH_4 ratio of 1:1, illustrating the clear difference in discharge characteristics for the empty reactor and the reactor with blank Al_2O_3 packing and WI Ni or Co catalyst, on the one hand, and with the various SC catalysts (most significant for Co), on the other hand. Especially the SC Co catalysts yield a significantly deformed Lissajous figure, indicating an increased effective dielectric capacitance ζ_{diel} .

packed DBD, yet even for this less complicated system, the precise underlying mechanisms remain unclear [66]. Therefore, further fundamental research is necessary to fully elucidate the relevant processes in a DBD to enable a complete understanding of how packing materials can affect the plasma discharge.

Similar to the I-V characteristics, the Lissajous figures show great variance depending on the catalyst material (or empty reactor), as shown in Fig. 6 for DRM and in Fig. 7 for NH_3 synthesis. Especially the SC (Co) catalysts yield an elongated Lissajous figure, which is more inclined upwards compared to e.g. the empty reactor. This indicates an increase of the effective dielectric capacitance ζ_{diel} (cf. Fig. 2 above), as more charge is stored by the dielectric for the same applied voltage [40]. Since the actual dielectric layer is identical for all experiments, this increased capacitance ζ_{diel} indicates a higher discharging areal fraction β , since a larger fraction of the dielectric now actually participates in the plasma discharge. In practice, this means that a larger part of the reactor volume is filled with plasma. This will be illustrated in Section 3.3 below, namely in Fig. 8B, D for DRM and in Fig. 10B, D, F for NH_3 synthesis, where especially for the SC Co catalysts the values of β are close to 1. The same is true for the SC Ni 3.3 wt% catalyst in case of NH_3 synthesis, also in line with the Lissajous plots of Fig. 7. When comparing the Lissajous figures from the different reactions, the dissimilarity between the shapes corresponding to the empty reactors stands out. The Lissajous figures from the empty reactor during NH_3 syntheses are notably less regular, exhibiting significant dips in the voltage. This is caused by the very high intensity of the microdischarges during this reaction in an empty reactor (as also visible in Fig. 5, note the deviant y-scale for the empty reactors) which very quickly add/remove charge from the dielectric, briefly affecting the measured voltage. We expect the higher breakdown voltage of N_2 to cause the increase in intensity of the microdischarges, as this means a higher electric field, and thus a higher charge on the dielectric, is required to initiate the discharge.

As described in Section 2.4, these I-V curves and Lissajous figures can be analyzed in detail to extract (semi-)quantitative information about the plasma discharge. The results for the microdischarge quantity and

discharging areal fraction β are presented in Fig. 8B, D for DRM and in Fig. 10B, D, F for the NH_3 synthesis experiments, and will be discussed in Section 3.3, to correlate them with the performance metrics. In addition, the burning voltage U_b , peak-to-peak applied voltage $U_{\text{pk-pk}}$, conductively transferred charge ΔQ_{dis} , and cell capacitance C_{cell} are presented and discussed in the SI (Section S11, Figs. S20–S29).

An intriguing observation is the behavior of the WI Co catalysts. As described earlier, this catalyst completely eliminates the formation of microdischarges (without affecting the plasma power, discussed in more detail in Section 3.3), as is also confirmed by the microdischarge quantity (see Fig. 8B, D and Fig. 10B, D, F in Section 3.3 below). However, for all other discharge characteristics, such as the discharging areal fraction β , the burning voltage U_b or the conductively transferred charge ΔQ_{dis} , the WI Co catalyst performs seemingly identical to the WI Ni catalyst or even blank Al_2O_3 , in stark contrast to especially the SC Co catalysts. This discrepancy between the microdischarge quantity and the other discharge characteristics for the WI Co catalysts suggests that the formation of microdischarges is governed by different mechanisms than those that affect the other discharge characteristics. The strongly affected Lissajous figures and subsequent discharge characteristics in the SC (Co) case also indicate an increased cell capacitance C_{cell} (see SI, Section S11, Figs S21, S23, S25, S27, and S29). We attribute this to the metallic layer at the surface of the dielectric beads. This metal/dielectric combination seems to turn these beads into small capacitors, naturally increasing the overall capacitance of the system. We hypothesize that this increased capacitance contributes to the altered plasma discharge, in particular the strong increase of the discharging areal fraction β and the characteristics that are connected to it. Further, this metallic layer strongly enhances the conductivity of the packing, which could allow for the higher conductively transferred charge at the lower burning voltages (see SI, Section S11). The burning voltage represents the gap voltage at the places where discharges are occurring, and therefore impacts the local electric field and ion/electron energies, though determining the latter is not straightforward [40]. This would also explain the behavior of the WI Co catalysts compared to the SC ones, since the WI beads

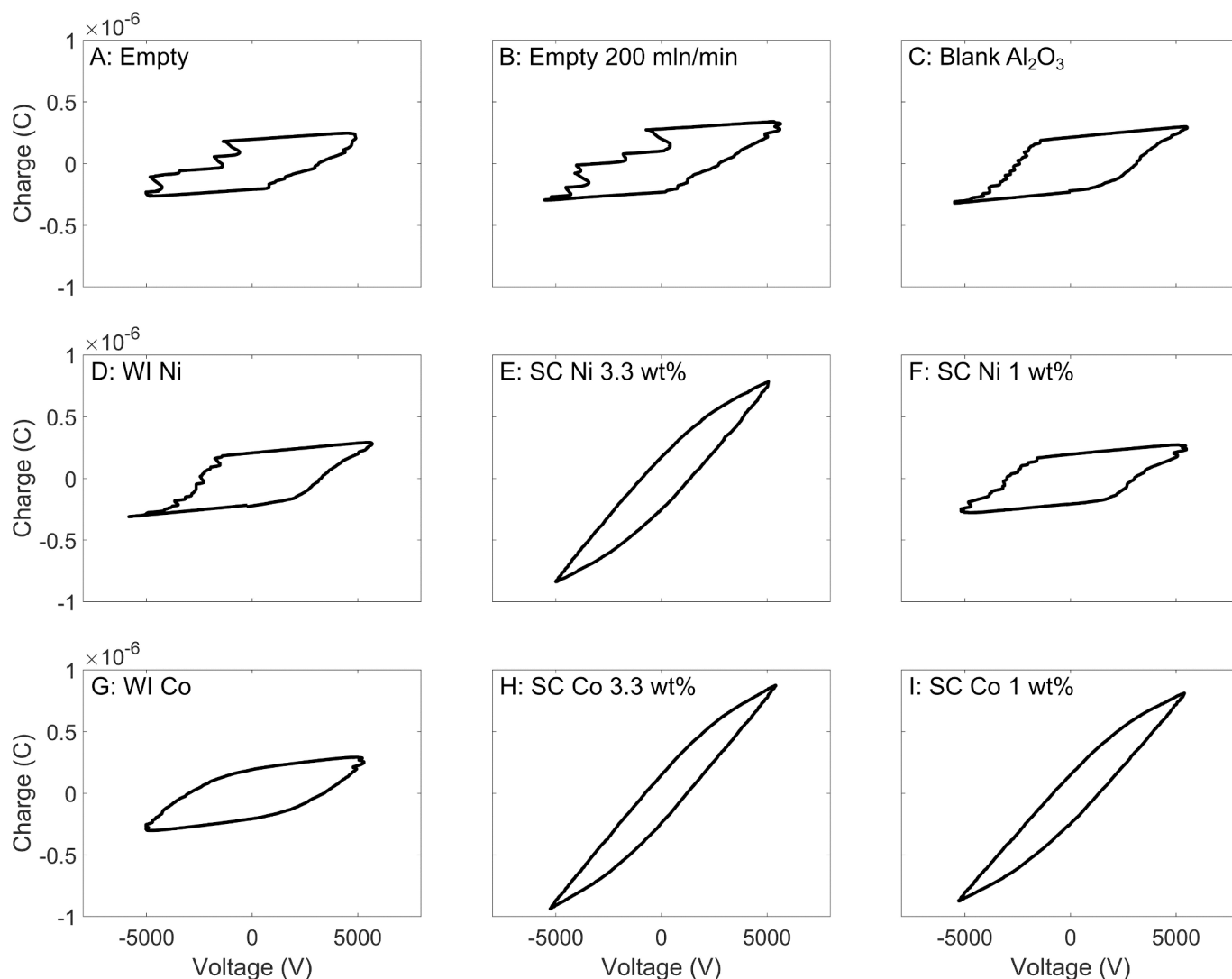


Fig. 7. Representative Lissajous figures for all experimental sets of NH_3 synthesis for a N_2/H_2 ratio of 1:1, illustrating the clear difference in discharge characteristics for the empty reactor and the reactor with blank Al_2O_3 packing and WI Ni or Co catalyst, on the one hand, and with the various SC catalysts, on the other hand. Especially the SC Co and SC Ni 3.3 wt% catalysts yield a significantly deformed Lissajous figure, indicating an increased effective dielectric capacitance ϵ_{diel} . The discrepancy for the SC Ni 1 wt% catalyst is again attributed to instability of the catalyst; see text.

exhibit metal particles at the surface (strongly decreasing the microdischarge quantity), but the particles do not form a layer at the surface, preventing charges to spread across the surface (and thus limiting the capacitance). Given the different underlying physical mechanisms that affect the microdischarges and the other discharge characteristics (e.g., partial discharging), these characteristics should always be considered separately and one of them cannot act as a representative measure for the others.

Another interesting observation is the very similar behavior of the WI Ni catalysts compared to blank Al_2O_3 . Despite having a 10 wt% metal loading (of which a part is not fully reduced, see SI Fig. S16), the WI Ni catalysts do not seem to alter the plasma discharge in a meaningful way. The contrast with the WI Co is striking, and most likely due to the lower surface coverage of the Ni particles on the WI Ni catalysts, compared to the Co samples (see Fig. 3B and C). On the one hand, this supports our hypothesis that metal particles exposed to the plasma can have a significant influence on the plasma discharge. On the other hand, this result implies that the effect of the catalyst on the plasma (compared to a support-only packing) can be reduced significantly, perhaps even eliminated, when the amount of metal particles at the outer surface of the support beads/pellets is sufficiently low. Furthermore, this

illustrates that the total metal loading of the catalyst can be relatively nondescriptive, especially when the distribution of the metal varies. This is also why the WI and SC catalysts are not compared at the same loading, since decreasing the loading of the WI Ni catalyst which already has limited effects does not make sense, and the higher loading for the SC catalysts was not structurally stable, as discussed in Section 2.1.

The clear change in discharge regime for the WI Co and the various SC catalysts, i.e., fewer and/or less intense microdischarge filaments (if any) than in the empty reactor or with blank Al_2O_3 packing, is also visualized by additional observations made using a quartz tube as the dielectric, illustrating the altered discharge behavior. The quartz tube enabled direct observation of the plasma, which is shown in the SI (Section S11, Fig. S19) for an empty reactor, one packed with blank Al_2O_3 and one with the SC Co 3.3 wt% catalyst. These pictures help illustrate the drastic change in discharge regime when comparing the empty and blank Al_2O_3 packed reactor to the reactor filled with SC catalyst. For the empty reactor, clear filamentary discharges are observed, which moved around freely as the plasma was ignited. For the blank Al_2O_3 packing, the discharge was still clearly filamentary, indicated by the bright spots in between the beads. In contrast, for the SC Co 3.3 wt% catalysts, the reactor was completely filled with a more uniform

plasma.

It must be noted that due to the practical limitations (e.g., the diameter of the quartz tube, etc.), the tests with the quartz tube could not be used for quantitative measurements and were only conducted as an illustrative example of the change of the discharge regime. Further, these simple pictures cannot be interpreted in a scientifically relevant way, and are shared merely to make the changes in the discharge more tangible and visible for the reader.

3.3. Plasma-catalytic performance and effect of the discharge characteristics

3.3.1. Dry reforming of methane

The total conversion of CO_2 and CH_4 is shown in Fig. 8A and C, together with the measured plasma power for an empty reactor, an empty reactor with a total flow rate of 200 mln/min to mimic the residence time of a packed reactor, and for a packed reactor with blank Al_2O_3 and with the various catalysts.

The first striking observation is that for the CO_2/CH_4 ratio of 1:1 (Fig. 8A), the total conversion is the highest for the empty reactor, which performed nearly identical to the reactor with blank Al_2O_3 beads. The SC Co catalysts only have a slightly lower conversion, while all other catalysts show a clear decrease in conversion. Indeed, microdischarges are expected to contribute to the overall CO_2 and CH_4 conversion, as demonstrated by previous chemical kinetics modeling from our group [67], and the microdischarge quantity is the highest for the empty reactor and the reactor packed with blank Al_2O_3 , while it drops significantly for all catalysts (except WI Ni); see Fig. 8B. Besides, the more intense microdischarges in the empty reactor (see also Fig. 4A) may also locally heat the gas to a higher temperature, which could further contribute to the increased conversion. On the other hand, the increased plasma volume for the SC Co catalysts (high β , see also Fig. 8B) could compensate for the lower microdischarge quantity, leading to a comparable overall conversion. The combination of a low microdischarge

quantity with a low discharging areal fraction β generally leads to poor performance in DRM (e.g. SC Ni 1 wt%). In the 200 mln/min case, the higher flow rate corresponds to a lower SEI (since the plasma power remained constant). The lower total conversion at this higher flow rate corresponds roughly to the decrease in SEI (i.e., a factor of 2), which leads to a nearly identical energy cost (see SI, Section S12, Fig. S30). This quasi-linear dependence of the conversion to the SEI indicates that in the case of the empty reactor, the overall performance is limited by the amount of energy that can be used for the forward reactions. Further, the plasma power remains nearly constant over all experiments, thus it cannot explain the stark differences in total conversion.

For the CO_2/CH_4 ratio of 2:1 (Fig. 8C), the SC Co catalysts outperform the blank Al_2O_3 and perform similarly to the empty reactor at the same flow rate, but clearly better than the empty reactor at the same residence time (flow rate of 200 mln/min). It is, however, not clear whether this improvement is due to a chemical catalytic effect, or simply due to a plasma (physical) effect, as it may again be explained by the larger plasma volume (high β , see Fig. 8D).

Importantly, the plasma-deposited power remained virtually constant regardless of the quantity of microdischarges (see Fig. 8A and C). Therefore, the changes in the conversion cannot be (partially) attributed to possible changes in power, but instead should be related to the properties of plasma. Given the similar thermal properties for all packed-bed experiments (i.e., the same gas flow rate, the same plasma power, the same reactor body through which heat can transfer and escape), we expect the overall temperature to be comparable for all experiments. However, the filamentary discharges are most likely creating hotspots on the catalyst, the dielectric, and in the gas, while the more homogeneous discharges will dissipate the heat more uniformly throughout the entire bed. Note that further insights can also be obtained from the temperature inside the plasma and the catalyst bed. However, measuring the temperature in plasma catalysis is very challenging. Introducing a temperature probe in the catalyst bed (i.e., the plasma discharge zone) would affect the plasma itself, which would then

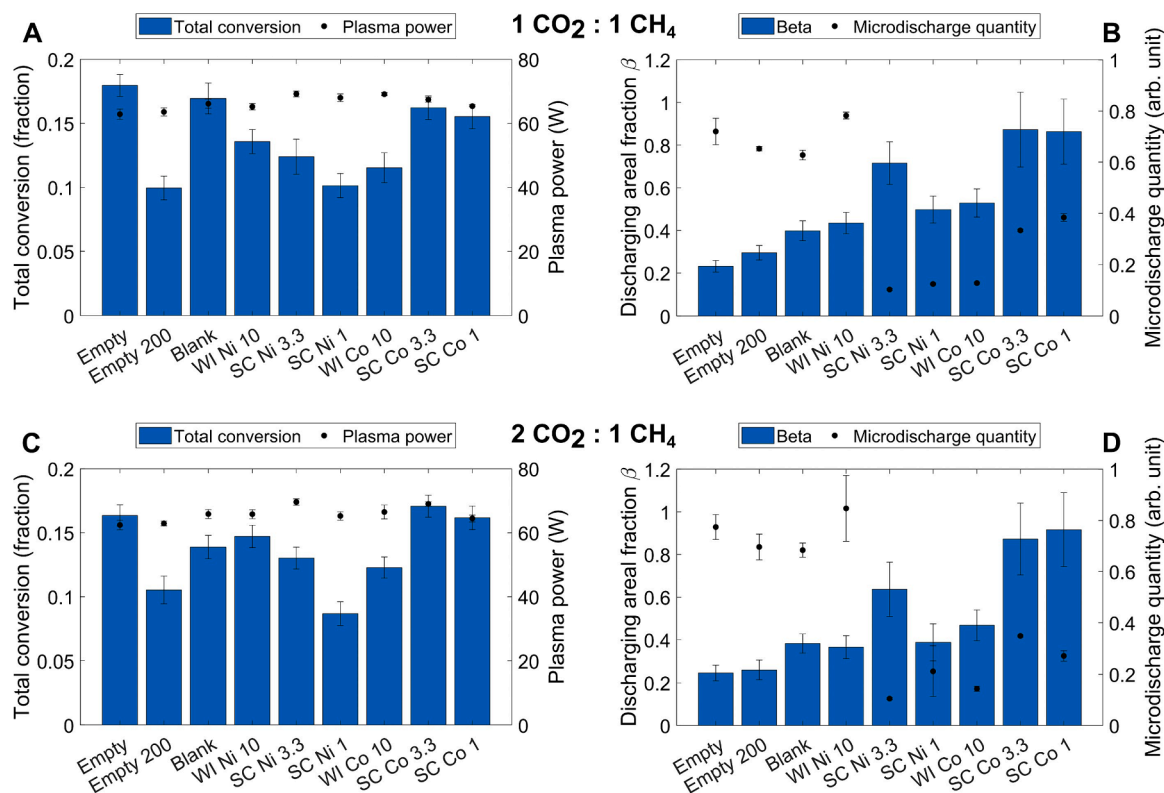


Fig. 8. Total conversion and measured plasma power for the various catalysts used for DRM with a CO_2/CH_4 ratio of 1:1 (A) and 2:1 (C). Discharging areal fraction β and microdischarge quantity for DRM with a CO_2/CH_4 ratio of 1:1 (B), and 2:1 (D).

yield wrong results, and it could damage the temperature probe. Measuring the gas temperature downstream would only give a very approximate temperature, as the gas cools down as soon as it exits the plasma zone. Alternatively, measuring the exterior of the reactor provides little insight in the true temperature of the catalyst bed, because the dielectric barrier is typically a poor thermal conductor as well, making the correlation between the outer and the inner temperature of the reactor difficult. To determine the true temperature at the catalyst surface itself, advanced techniques and dedicated setups are required [68–70], which cannot readily be coupled with conventional plasma catalysis experiments.

Altogether, the highest conversion appears to be correlated to either a high microdischarge quantity (i.e., many microdischarge filaments, and/or with high intensity), or a high discharging areal fraction β (i.e., large fraction of reactor volume filled with plasma), and thus, plasma (physical) effects, while chemical catalytic effects are not clearly demonstrated. However, even though our results do not directly indicate chemical effects, a contribution of plasma-catalytic reactions cannot be excluded. As discussed by Loenders et al., plasma-catalytic reactions can be counterproductive in DRM [8]. Indeed, modeling predicts that the plasma-produced radicals may be quenched at a (transition metal)

catalyst surface, and react back into the reactants, rather than into the products. This may add to the physical effects that were already discussed, leading to the poor overall performance as observed here [8]. In order to gain further insights into the contributions of plasma-catalytic reactions (metal surface reactions, specifically), a meticulous approach as presented by Barboun et al. would be required [71]. There, a distinction is made between plasma-phase and surface-catalytic reactions in plasma-assisted NH_3 synthesis. Despite offering valuable insights, their approach is not directly applicable here, since the plasma discharge differs significantly between the metal-loaded and blank supports. Furthermore, the distribution of the metal particles on and throughout the support is complex, hindering the rational interpretation of accessible metal-site measurements (e.g., CO-chemisorption, as presented by Barboun et al.).

Nevertheless, we don't make a direct comparison between thermal and plasma catalysis in this work. Indeed, this has been often performed in literature, and can sometimes provide additional insights. However, it is also becoming increasingly clear that plasma catalysis cannot be simply described as "thermal catalysis with additional complexity" [8,34,35,45]. There is no direct correlation between the performance of certain catalysts in thermal versus plasma catalysis. Therefore, we

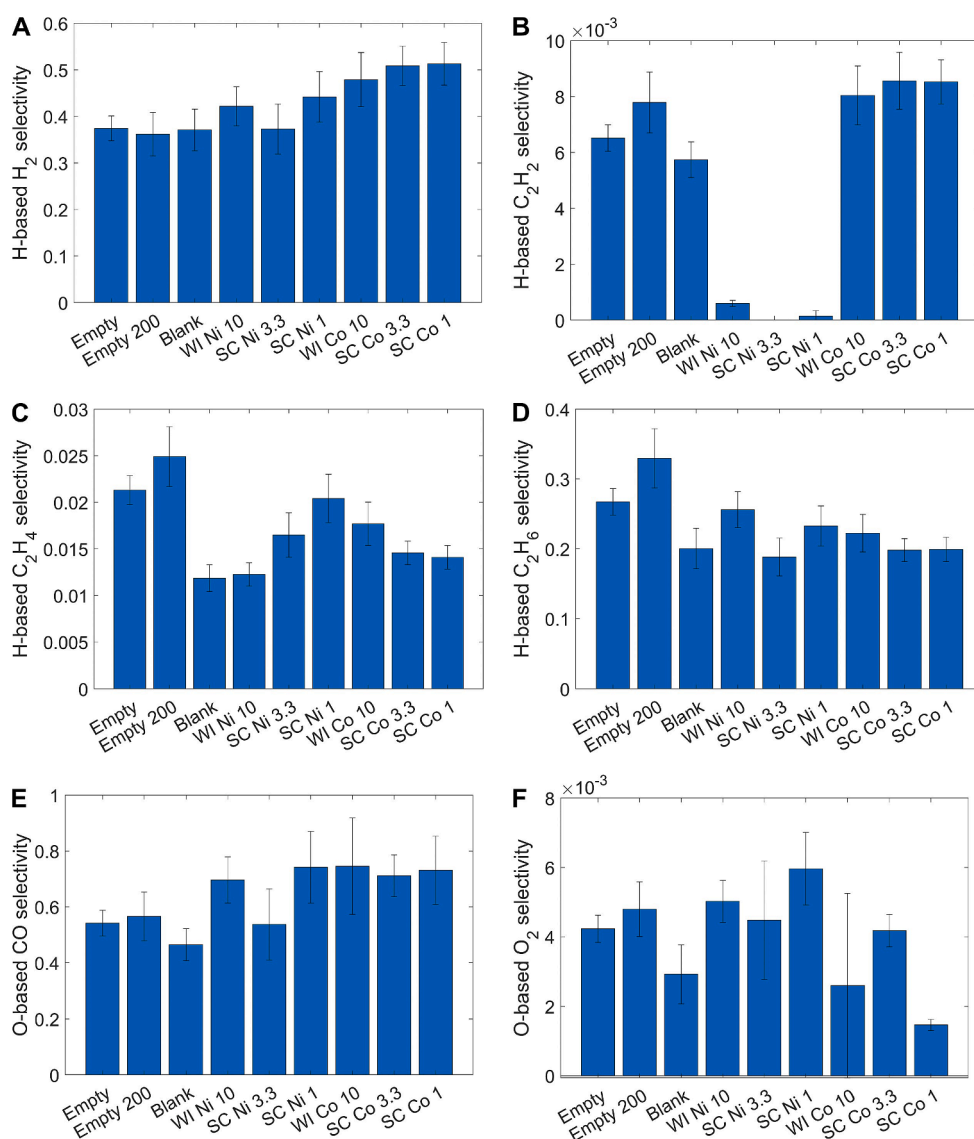


Fig. 9. Selectivities based on DRM experiments with a CO_2/CH_4 ratio of 1:1. A: H-based H_2 selectivity. B: H-based C_2H_2 selectivity. C: H-based C_2H_4 selectivity. D: H-based C_2H_6 selectivity. E: O-based CO selectivity. F: O-based O_2 selectivity.

believe our work challenges this conventional paradigm, stressing the complexity and uniqueness of plasma catalysis, requiring a dedicated approach, independent from thermal catalysis, to achieve novel insights.

The presence of plasma-catalytic reactions is further supported by the selectivities, since the various catalysts do affect the selectivities towards various products. All selectivities are presented in the SI (Section S12, Figs. S33–S35), while the most relevant ones are shown in Fig. 9. Firstly, the H₂ selectivity is either similar or increased for the metal-loaded beads compared to the blank Al₂O₃. Similar observations were made by Tu et al., where a drop in total conversion combined with a higher H₂ selectivity was observed for a Ni/Al₂O₃ catalyst in DRM compared to plasma-only [22]. Further, the changes in the selectivities towards C₂H₂, C₂H₄ and C₂H₆ are remarkable. For all Ni-containing catalysts, virtually no C₂H₂ was formed, while for the Co-containing catalysts, the C₂H₂ selectivity was higher than for the empty reactor or the one packed with blank Al₂O₃. This implies that the formation of C₂H₂ is less dependent on the discharge, but that indeed, a catalytic effect is dominant here, where Co clearly outperforms Ni. However, the underlying mechanism for this is still unclear and would require more detailed catalyst characterization or *in-situ* diagnostics, which is outside the scope of the present paper. DFT simulations of the catalyst surface, combined with microkinetic modelling, could offer further fundamental insights into the underlying mechanisms of this apparent surface catalytic effect [72]. The C₂H₄ and C₂H₆ selectivities for the various catalysts are generally similar or lower compared to the empty reactor. This suggests a stronger dependence on the discharge, rather than any catalytic effects. In addition, the O-based selectivities (see Fig. 9E and F) show some variance as well. For the CO₂/CH₄ ratio of 1:1, the SC Ni 1 wt % and Co catalysts show the highest combined O-based selectivity, implying that a lower amount of liquid components (mostly H₂O, see above) were formed (as they are not included in this (gas-phase) O-based selectivity). This suggests that the overall chemistry is affected compared to the other experiments, though given the relatively large error bars, it is hard to draw direct conclusions.

Despite the increasing number of works on plasma-catalytic DRM, the observations reveal discrepancies which make isolating any trends difficult. For example, similar to our observations, Tu et al. found that when introducing a Ni/Al₂O₃ catalyst, the total conversion decreases, which they also attributed to alterations of the plasma discharge [22]. Though, they also observed a dramatic increase in H₂ selectivity, which was less distinct in our experiments. Similarly, Brune et al. saw little to no changes in conversion when introducing a Ni/Al₂O₃ or Co/Al₂O₃ catalyst, despite minor changes in the plasma discharge [24]. Contrastingly, Farshidkroh et al. did see an increase of the total conversion, but the driving mechanisms remain unclear [17]. Similarly, Suttikul et al. saw a clear increase in total conversion when introducing Ni to the Al₂O₃ support, which they attributed to catalytic effects [21]. However, the relevant discharge characteristics were not reported, so it remains ambiguous as to what role the discharge plays in these seemingly catalytic effects. We believe that the discharge characteristics could indeed play an important role in these observations, and clear analyses and reporting are crucial to gain a complete understanding of the plasma-catalytic performance.

In short, while the DRM performance is clearly affected in different ways by the multiple catalysts, the observed differences in performance cannot be attributed simply to catalytic effects in the conventional sense. Various discharge characteristics, not in the least the microdischarges, will influence the gas-phase chemistry, which can have significant effects on the overall performance. It is therefore essential to always take discharge characteristics into account when comparing different catalysts or packing materials. Interpretation of data should be done with caution, making sure discharge effects are identical before attributing performance changes to precisely defined catalytic mechanisms.

3.3.2. NH₃ synthesis

In contrast to DRM, the beneficial effect of the catalysts is much

clearer in NH₃ synthesis; see Fig. 10A, C, E. In general, all SC catalysts (except SC Ni 1 wt%, most likely due to its instability, see earlier discussion) perform significantly better than the WI catalysts, the blank Al₂O₃ and the empty reactor. While for an N₂/H₂ ratio of 1:1 the Al₂O₃ packing already increases the NH₃ concentration by a factor of 2 compared to the empty reactor, and the WI catalysts perform even slightly better (WI Ni 2.5 times higher and WI Co 3 times higher), the SC Ni 3.3 wt% and the SC Co catalysts enhance the NH₃ concentration by a factor of over 5. The significant alteration of the plasma discharge by the SC catalysts (which makes it much more homogenous and expanded instead of filamentary, as indicated by the nearly doubling of the discharging areal fraction β and by the microdischarge quantity decreasing by a factor of more than 2, see Fig. 10), drastically improves the NH₃ synthesis. This is again in line with earlier chemical kinetics simulations by our group, which predicted that NH₃ is largely destroyed in the microdischarge filaments [10], as well as by previous experimental studies [11,35,36]. In other words, fewer (and less intense) microdischarges will improve the NH₃ synthesis. Potentially, the intense filaments in the empty reactor locally heat the gas volume of the filaments substantially, contributing to the decreased NH₃ production due to thermal decomposition of the formed NH₃. In the altered discharge, these fewer and/or less intense microdischarges may locally heat the gas less, rather spreading the heat uniformly across the reactor volume. The lack of hotspots could contribute to the increased overall performance due to the lower rate of thermal NH₃ decomposition.

The case of the WI Co catalyst is again an intriguing one. For the N₂/H₂ ratio of 3:1 (and also the 1:1 ratio, although less pronounced), it performs somewhere in-between the SC catalysts and the blank Al₂O₃/WI Ni catalysts. As discussed earlier, the WI Co catalyst eliminated the microdischarges, which is an evident benefit for NH₃ synthesis, as explained above [10]. However, the lack of microdischarges cannot be the only parameter influencing the NH₃ production, since the SC Co and SC Ni 3.3 wt% still clearly outperform the WI Co, even though the microdischarge quantity is not lower when using these SC catalysts. Two other main mechanisms, besides the rather low microdischarge quantity, may cause this clear improvement by the SC catalysts. Firstly, the plasma is more expanded, filling the reactor entirely (as is indicated by the discharging areal fraction β being close to 1, see Fig. 10B, D, F), thus increasing the overall plasma volume. This larger plasma volume increases the effective residence time, since the gas is exposed to plasma throughout the entire reactor volume, rather than just in the discrete filaments. At the same time, since the plasma power remains constant, the local power density will be lower. This should enable an overall larger NH₃ synthesis, because the higher power density facilitates the decomposition of the formed NH₃ more than its synthesis, as was predicted by modeling [10]. Secondly, the SC catalysts generally expose more metal surface to the plasma, potentially enabling a more pronounced catalytic effect in the conventional sense, although the latter would require further investigation to really prove this hypothesis.

Interestingly, the benefit of the WI Co catalyst over Al₂O₃ and WI Ni is no longer present at a N₂/H₂ ratio of 1:3. This implies that at this stoichiometric ratio, the destruction of NH₃ in the microdischarge filaments may no longer hinder the performance. Rather, the amount of activated N₂ is expected to be too low compared to the activated H₂, as the latter is much more readily activated by plasma given its much lower bond dissociation energy. The lower NH₃ production is expected to be a more dominant factor compared to the destruction of NH₃ for the N₂-richer ratios. The best performance being obtained with a N₂/H₂ ratio of 1:1 is again attributed to the higher activation energy of N₂ compared to H₂, making the stoichiometric gas mixture less effective [34]. Note that the highest performance of 14570 ppm NH₃ at 100 mln/min with a N₂/H₂ ratio of 1:1 corresponds to a N₂ conversion of 1.4 %, and an energy cost of 60 MJ/mol. This is still far from competing with Haber-Bosch, which very well may never be achievable for direct plasma-catalytic NH₃ synthesis. Other options, e.g., based on NO_x production by warm plasmas (which is much more energy-efficient), followed by the

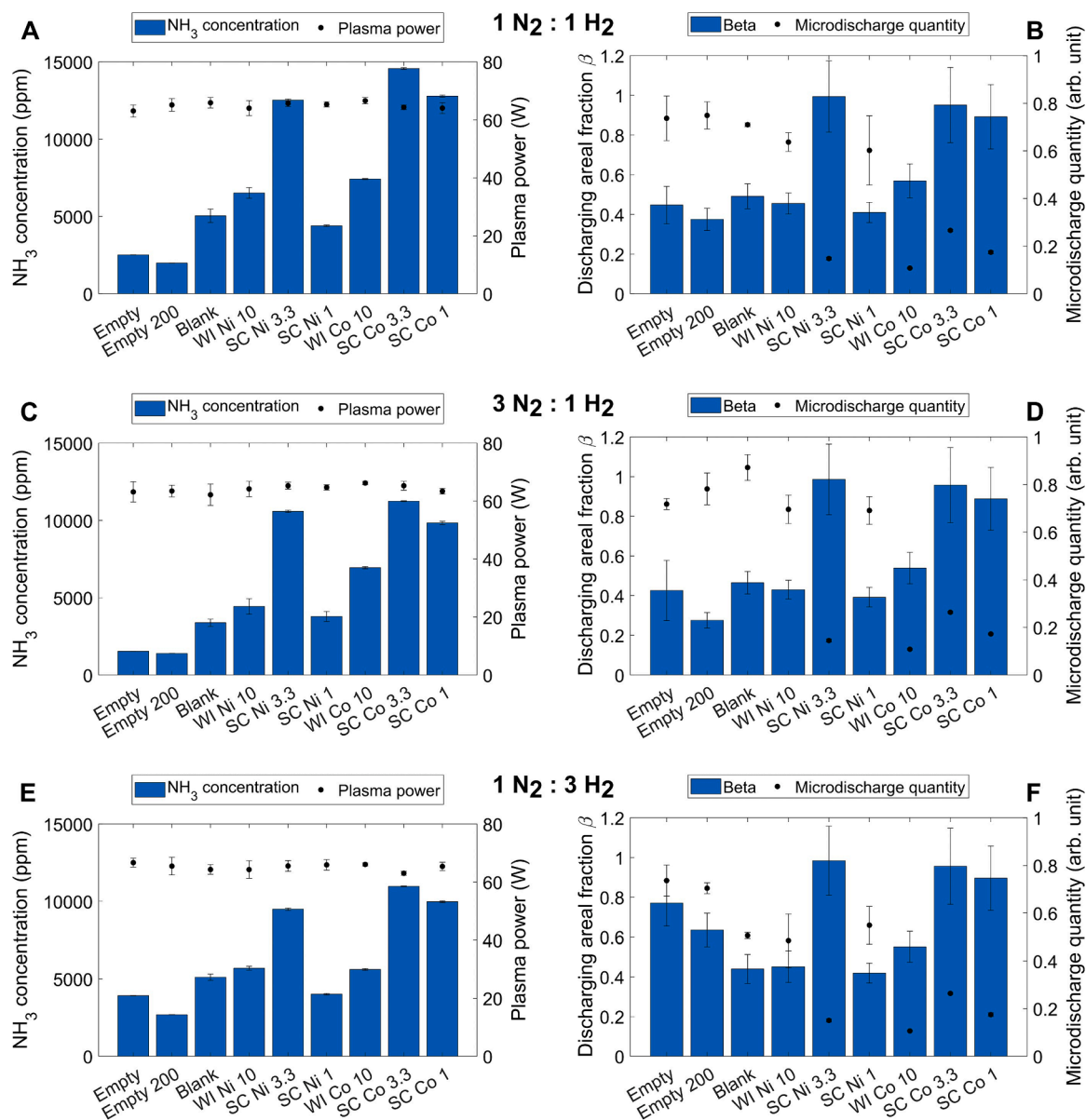


Fig. 10. NH₃ outflow concentration and measured plasma power for a N₂:H₂ ratio of 1:1 (A), 3:1 (C), and 1:3 (E). Discharging areal fraction β and microdischarge quantity for a N₂:H₂ ratio of 1:1 (B), 3:1 (D), and 1:3 (F).

catalytic reduction into NH₃ [73] are more promising in this respect. However, reaching the best performance is not the aim of this work, as we rather aspire to better understand plasma catalysis on a fundamental level.

Indeed, we want to stress the importance of the gas-phase plasma reactions, and how the packing/catalyst can affect those, indirectly altering the overall performance. Also in literature, it was reported that catalysts do not always have a beneficial effect on the reaction. For DRM, for example, it was recently proposed [8] that transition metal catalysts could even have a negative effect on the overall performance, because they can quench the plasma radicals, and let them react back to the reactants instead of towards the desired products. Further, for plasma-catalytic NH₃ synthesis, modeling work [74] suggests that the actual catalyst metal has little effect on the overall performance, when radicals play a dominant role (as is mostly the case in DBD plasma), which was further supported by experimental work [45].

3.3.3. Importance of the discharge characteristics

Inherently, plasma catalysis is complicated, with many aspects to

take into account. In addition to the relevant parameters and mechanisms in more conventional heterogeneous catalysis, such as the physical and chemical properties of the catalyst (nano)particles and support materials, the plasma discharge cannot be neglected here. Not only is the plasma an indispensable part of the system, it is highly sensitive to many external factors, not in the least to the packing material (i.e., the catalyst). It is therefore impossible to treat the plasma discharge as an independent “constant parameter” in an experimental setup, without thorough analysis and comparison.

The complexity of these systems is also illustrated by seemingly contradictory results. For example, Andersen et al. found that microdischarges are detrimental for NH₃ synthesis, and are in fact beneficial for NH₃ decomposition [11,36]. These findings are in line with earlier model predictions from our group [10], and with our observations in this work, where a lower microdischarge quantity tends to correspond to a higher NH₃ yield. On the other hand, Patil et al. reported that microdischarges are beneficial for NH₃ synthesis [29,34]. It is not straightforward to pinpoint the underlying cause of this discrepancy. However, it illustrates that many parameters need to be taken into

account and further fundamental research is required to fully elucidate what mechanisms drive plasma catalysis in DBDs, especially in packed-bed configurations.

In practice, it is crucial to monitor the plasma discharge using the conventional electrical diagnostics. Further, a quantification of the discharge characteristics is highly advisable, since not all discharge characteristics are immediately visually obvious. Only when it is confirmed that the plasma discharge is identical for two different catalysts, it is possible to confidently attribute any changes in overall performance to catalytic effects. Whenever there are discrepancies in the discharge, even if they seem minor, caution is advised when interpreting the results, as gas phase chemistry can be dominant, even in so-called plasma catalysis.

An additional takeaway of this work is that when studying different catalysts, simply applying the same synthesis protocol for different (metal) precursors may not suffice, as we illustrated here by the WI Ni and WI Co catalysts. A thorough, spatially resolved microscopic characterization of the catalysts is strongly advised. Ideally, this additional analysis goes beyond the conventional catalyst characterization techniques that are commonly applied for thermal catalysis, but lack spatial information on the support (such as XRD, N₂ sorption, etc.).

In short, we studied here both DRM and NH₃ synthesis, showing vastly different responses to changes in the plasma discharge. DRM seems to benefit from the presence of (more, stronger) microdischarge filaments, as they give rise to higher CO₂ and CH₄ conversion (in line with model predictions [67]). For NH₃ synthesis, we observe the opposite effect, since a better performance is gained with more uniform discharges, as created by the SC catalysts, because the microdischarge filaments destroy the formed NH₃, as also elucidated by model predictions [10]. Therefore, it is clear that every reaction or gas mixture will react differently to changes in the discharge properties. Thus, especially when studying lesser-known reactions, the effect of the discharge on the specific reaction should be studied in greater detail, in order to be able to separate gas-phase chemistry from the desired catalytic reactions.

4. Conclusion

We performed a number of plasma catalysis experiments in a packed-bed DBD reactor for both DRM and NH₃ synthesis. We synthesized both Ni and Co on Al₂O₃ catalysts in two different ways, i.e., by wet impregnation (WI) and spray-coating (SC), yielding very different distributions of metal/metal oxide on and throughout the porous support beads. These changes in catalyst morphology had a drastic impact on the plasma discharge, in some cases eliminating the formation of microdischarges, and thus forming a more homogeneous plasma, filling the entire reactor. We also found that not all characteristics are impacted by the same catalysts, indicating that different mechanisms govern the various properties of the plasma discharge. Specifically, the microdischarges were eliminated by the WI Co catalyst (exhibiting a relatively high coverage of nanoparticles at its surface), without displaying the fully expanded plasma that was observed for the SC catalysts (which have a μm-scale layer of metal nanoparticles at their surface).

Even when the same metal was deposited on the same support, but with a different synthesis method that distributed the metal differently on/throughout the support, the various catalysts showed great variety in overall performance. Especially for NH₃ synthesis, the benefit of the SC catalysts over the WI catalysts was tremendous. This strong improvement is attributed to the altered plasma discharge, which fills a larger part of the reactor volume, promoting the formation of NH₃, while at the same time limiting the destruction of the formed NH₃ due to the lower microdischarge quantity. For DRM, the influence of the discharge on the overall performance was more ambiguous, but also here the plasma discharge affects the performance. Especially the presence of microdischarges and a larger plasma volume (larger discharging areal fraction) seem beneficial for the overall DRM reaction. By studying these

dissimilar chemistries, we aim to illustrate how plasma properties and their effect on the performance do not translate well between various reactions.

Though the precise SC synthesis as described here needs further optimization, given the unstable nature of the metallic shell (as demonstrated for SC Ni 1 wt%), the general conclusions offer an interesting perspective. By deliberately designing the packing of the reactor in such a way, the plasma could be altered relatively easily to tune its properties towards the desired form (i.e. diffuse rather than filamentary). Further optimization can be done to design a robust packing that resembles the presented beads, i.e., a dielectric core with a thin metallic shell. This can serve as a template to add further catalytically relevant materials, to aim for a desired combination of the altered plasma discharge and other proposed beneficial mechanisms. This core-shell structure could further serve as a simple and reliable plasma modifier to study the effect of the plasma discharge on other reactions of interest. Further, this could aid fundamental studies looking into the mechanisms that govern (packed-bed) dielectric barrier discharges, as the precise underlying mechanisms are still poorly understood.

We hope our findings are interesting, not only for the plasma catalysis field, but also the entire catalysis community. Indeed, more and more (classical) catalysis groups are starting research on plasma catalysis as well, due to the large benefits of plasma (catalysis) for electrifying chemical reactions. It is important for thermal catalysis researchers to realize that plasma catalysis is more complex than thermal catalysis, because introducing a (catalytic) packing in the reactor inevitably affects the plasma. As presented here, small changes in that packing can sometimes have drastic implications with regard to the plasma behavior. When studying and comparing different catalysts, it is therefore crucial to measure, analyze, and report the discharge characteristics for all experiments. Given the general complexity of plasma catalysis, due to the vast variety in both chemical and physical effects that can take place, extra care should be taken when interpreting the results from plasma-catalytic tests. Only when it is clear that certain changes in performance cannot be attributed to differences in plasma behavior, it is possible to hypothesize purely catalytic mechanisms to understand the observed results.

CRedit authorship contribution statement

Robin De Meyer: Writing – review & editing, Writing – original draft, Visualization, Validation, Software, Methodology, Investigation, Formal analysis, Data curation, Conceptualization. **Yury Gorbaney:** Writing – review & editing, Validation, Supervision, Methodology, Investigation, Conceptualization. **Radu-George Ciocarlan:** Writing – review & editing, Validation, Supervision, Methodology, Investigation, Formal analysis, Conceptualization. **Pegie Cool:** Writing – review & editing, Supervision, Methodology, Funding acquisition, Conceptualization. **Sara Bals:** Writing – review & editing, Supervision, Funding acquisition. **Annemie Bogaerts:** Writing – review & editing, Supervision, Methodology, Funding acquisition, Conceptualization.

Declaration of competing interest

The authors declare the following financial interests/personal relationships which may be considered as potential competing interests: Annemie Bogaerts reports financial support was provided by European Research Council. Sara Bals reports financial support was provided by European Research Council. Annemie Bogaerts reports financial support was provided by University of Antwerp. If there are other authors, they declare that they have no known competing financial interests or personal relationships that could have appeared to influence the work reported in this paper.

Data availability

Data will be made available on request.

Acknowledgments

This research was supported through long-term structural funding (Methusalem FFB15001C) and by the European Research Council (ERC) under the European Union's Horizon 2020 research and innovation programme with grant agreement No 810182 (SCOPE ERC Synergy project) and with grant agreement No 815128 (REALNANO). We acknowledge the practical contribution of Senne Van Doorslaer.

Appendix A. Supplementary data

Supplementary data to this article can be found online at <https://doi.org/10.1016/j.cej.2024.150838>.

References

- [1] A. Bogaerts, X. Tu, J.C. Whitehead, G. Centi, L. Lefferts, O. Guaitella, F. Azzolina-Jury, H.-H. Kim, A.B. Murphy, W.F. Schneider, T. Nozaki, J.C. Hicks, A. Rousseau, F. Thevenet, A. Khacef, M. Carreon, The 2020 plasma catalysis roadmap, *J. Phys. Appl. Phys.* 53 (2020) 443001, <https://doi.org/10.1088/1361-6463/ab9048>.
- [2] Y. Zeng, X. Zhu, D. Mei, B. Ashford, X. Tu, Plasma-catalytic dry reforming of methane over γ -Al₂O₃ supported metal catalysts, *Plasmas Enhanc. Catal. Process. ISPCEM 2014 (256)* (2015) 80–87, <https://doi.org/10.1016/j.cattod.2015.02.007>.
- [3] M.L. Carreon, Plasma catalytic ammonia synthesis: state of the art and future directions, *J. Phys. Appl. Phys.* 52 (2019) 483001, <https://doi.org/10.1088/1361-6463/ab3b2c>.
- [4] R. Snoeckx, A. Bogaerts, Plasma technology – a novel solution for CO₂ conversion? *Chem. Soc. Rev.* 46 (2017) 5805–5863, <https://doi.org/10.1039/C6CS00066E>.
- [5] K.H.R. Rouwenhorst, Y. Engelmann, K. van 't Veer, R.S. Postma, A. Bogaerts, L. Lefferts, Plasma-driven catalysis: green ammonia synthesis with intermittent electricity, *Green Chem.* 22 (2020) 6258–6287, <https://doi.org/10.1039/D0GC02058C>.
- [6] K. Ollegott, P. Wirth, C. Oberste-Beulmann, P. Awakowicz, M. Muhler, Fundamental properties and applications of dielectric Barrier Discharges in plasma-catalytic processes at atmospheric pressure, *Chem. Ing. Tech.* 92 (2020) 1542–1558, <https://doi.org/10.1002/cite.202000075>.
- [7] X. Tu, H.J. Gallon, J.C. Whitehead, Electrical and spectroscopic diagnostics of a single-stage plasma-catalysis system: effect of packing with TiO₂, *J. Phys. Appl. Phys.* 44 (2011) 482003, <https://doi.org/10.1088/0022-3727/44/48/482003>.
- [8] B. Loenders, R. Michiels, A. Bogaerts, Is a catalyst always beneficial in plasma catalysis? insights from the many physical and chemical interactions, *J. Energy Chem.* (2023), <https://doi.org/10.1016/j.jechem.2023.06.016>.
- [9] R. Snoeckx, Y.X. Zeng, X. Tu, A. Bogaerts, Plasma-based dry reforming: improving the conversion and energy efficiency in a dielectric barrier discharge, *RSC Adv.* 5 (2015) 29799–29808, <https://doi.org/10.1039/C5RA01100K>.
- [10] K. van 't Veer, Y. Engelmann, F. Reniers, A. Bogaerts, Plasma-catalytic ammonia synthesis in a DBD plasma: role of Microdischarges and their afterglows, *J. Phys. Chem. C* 124 (2020) 22871–22883, <https://doi.org/10.1021/acs.jpcc.0c05110>.
- [11] J.A. Andersen, M.C. Holm, K. van 't Veer, J.M. Christensen, M. Østberg, A. Bogaerts, A.D. Jensen, Plasma-catalytic ammonia synthesis in a dielectric barrier discharge reactor: a combined experimental study and kinetic modeling, *Chem. Eng. J.* 457 (2023) 141294, <https://doi.org/10.1016/j.cej.2023.141294>.
- [12] G. Chen, J. Qu, P. Cheah, D. Cao, Y. Zhao, Y. Xiang, Size-dependent activity of iron Nanoparticles in both thermal and plasma driven catalytic ammonia decomposition, *Ind. Eng. Chem. Res.* 61 (2022) 11436–11443, <https://doi.org/10.1021/acs.iecr.2c02092>.
- [13] Y. Zhang, S. Li, Z. Yuan, H. Chen, X. Fan, Mechanochemical synthesis of RuCo/MgTiO₃ catalysts for nonthermal plasma-assisted ammonia synthesis, *Ind. Eng. Chem. Res.* 61 (2022) 14199–14210, <https://doi.org/10.1021/acs.iecr.2c02216>.
- [14] X. Zhu, X. Hu, X. Wu, Y. Cai, H. Zhang, X. Tu, Ammonia synthesis over γ -Al₂O₃ pellets in a packed-bed dielectric barrier discharge reactor, *J. Phys. Appl. Phys.* 53 (2020) 164002, <https://doi.org/10.1088/1361-6463/ab6cd1>.
- [15] K.H.R. Rouwenhorst, H.G.B. Burbach, D.W. Vogel, J. Núñez Paulí, B. Geerdink, L. Lefferts, Plasma-catalytic ammonia synthesis beyond thermal equilibrium on Ru-based catalysts in non-thermal plasma, *Catal. Sci. Technol.* 11 (2021) 2834–2843, <https://doi.org/10.1039/D0CY02189J>.
- [16] J.A. Andersen, J.M. Christensen, M. Østberg, A. Bogaerts, A.D. Jensen, Plasma-catalytic dry reforming of methane: screening of catalytic materials in a coaxial packed-bed DBD reactor, *Chem. Eng. J.* 397 (2020) 125519, <https://doi.org/10.1016/j.cej.2020.125519>.
- [17] Z. Farshidrok, M.R. Khani, A. Khodadadi, M. Gharibi, B. Shokri, Dry reforming of methane over Ni/ γ -MgO catalysts in a coaxial dielectric Barrier Discharge reactor, *Chem. Eng. Technol.* 44 (2021) 589–599, <https://doi.org/10.1002/ceat.202000455>.
- [18] A.H. Khoja, M. Tahir, N.A.S. Amin, A. Javed, M.T. Mehran, Kinetic study of dry reforming of methane using hybrid DBD plasma reactor over La₂O₃ co-supported Ni/MgAl₂O₄ catalyst, *Int. J. Hydrog. Energy* 45 (2020) 12256–12271, <https://doi.org/10.1016/j.ijhydene.2020.02.200>.
- [19] Y. Uytendhouver, K.M. Bal, E.C. Neyts, V. Meynen, P. Cool, A. Bogaerts, On the kinetics and equilibria of plasma-based dry reforming of methane, *Chem. Eng. J.* 405 (2021) 126630, <https://doi.org/10.1016/j.cej.2020.126630>.
- [20] L. Wang, Y. Wang, L. Fan, H. Xu, B. Liu, J. Zhang, Y. Zhu, X. Tu, Direct conversion of CH₄ and CO₂ to alcohols using plasma catalysis over Cu/Al(OH)₃ catalysts, *Chem. Eng. J.* 466 (2023) 143347, <https://doi.org/10.1016/j.cej.2023.143347>.
- [21] T. Suttikul, S. Nuchdang, D. Rattanaphra, C. Phalakornkule, Influence of operating Parameters, Al₂O₃ and Ni/Al₂O₃ catalysts on plasma-assisted CO₂ reforming of CH₄ in a Parallel plate dielectric Barrier Discharge for high H₂/CO ratio syngas production, *Plasma Chem. Plasma Process.* 40 (2020) 1445–1463, <https://doi.org/10.1007/s11090-020-10118-7>.
- [22] X. Tu, H.J. Gallon, M.V. Twigg, P.A. Gorry, J.C. Whitehead, Dry reforming of methane over a Ni/Al₂O₃ catalyst in a coaxial dielectric barrier discharge reactor, *J. Phys. Appl. Phys.* 44 (2011) 274007, <https://doi.org/10.1088/0022-3727/44/27/274007>.
- [23] W.-C. Chung, K.-L. Pan, H.-M. Lee, M.-B. Chang, Dry reforming of methane with dielectric Barrier Discharge and ferroelectric packed-bed reactors, *Energy Fuels* 28 (2014) 7621–7631, <https://doi.org/10.1021/ef5020555>.
- [24] L. Brune, A. Ozkan, E. Genty, T. Visart de Bocarmé, F. Reniers, Dry reforming of methane via plasma-catalysis: influence of the catalyst nature supported on alumina in a packed-bed DBD configuration, *J. Phys. Appl. Phys.* 51 (2018) 234002, <https://doi.org/10.1088/1361-6463/aac047>.
- [25] D. Mei, M. Sun, S. Liu, P. Zhang, Z. Fang, X. Tu, Plasma-enabled catalytic dry reforming of CH₄ into syngas, hydrocarbons and oxygenates: insight into the active metals of γ -Al₂O₃ supported catalysts, *J. CO₂ Util.* 67 (2023) 102307, <https://doi.org/10.1016/j.jcou.2022.102307>.
- [26] D. Mei, G. Duan, J. Fu, S. Liu, R. Zhou, R. Zhou, Z. Fang, P.J. Cullen, K. (Ken) Ostrikov, CO₂ reforming of CH₄ in single and double dielectric barrier discharge reactors: Comparison of discharge characteristics and product distribution, *J. CO₂ Util.* 53 (2021) 101703, <https://doi.org/10.1016/j.jcou.2021.101703>.
- [27] F. Gorky, J.M. Lucero, J.M. Crawford, B.A. Blake, S.R. Guthrie, M.A. Carreon, M. L. Carreon, Insights on cold plasma ammonia synthesis and decomposition using alkaline earth metal-based perovskites, *Catal. Sci. Technol.* 11 (2021) 5109–5118, <https://doi.org/10.1039/D1CY00729G>.
- [28] J. Hong, M. Aramesh, O. Shimoni, D.H. Seo, S. Yick, A. Greig, C. Charles, S. Praver, A.B. Murphy, Plasma catalytic synthesis of ammonia using functionalized-Carbon coatings in an atmospheric-pressure non-equilibrium Discharge, *Plasma Chem. Plasma Process.* 36 (2016) 917–940, <https://doi.org/10.1007/s11090-016-9711-8>.
- [29] B.S. Patil, A.S.R. van Kaathoven, F.J.J. Peeters, N. Cherkasov, J. Lang, Q. Wang, V. Hessel, Deciphering the synergy between plasma and catalyst support for ammonia synthesis in a packed dielectric barrier discharge reactor, *J. Phys. Appl. Phys.* 53 (2020) 144003, <https://doi.org/10.1088/1361-6463/ab6a36>.
- [30] S. Li, T. van Raak, F. Gallucci, Investigating the operation parameters for ammonia synthesis in dielectric barrier discharge reactors, *J. Phys. Appl. Phys.* 53 (2019) 014008, <https://doi.org/10.1088/1361-6463/ab4b37>.
- [31] J. Liu, X. Zhu, X. Hu, F. Zhang, X. Tu, Plasma-assisted ammonia synthesis in a packed-bed dielectric barrier discharge reactor: effect of argon addition, *Vacuum* 197 (2022) 110786, <https://doi.org/10.1016/j.vacuum.2021.110786>.
- [32] F.A. Herrera, G.H. Brown, P. Barboun, N. Turan, P. Mehta, W.F. Schneider, J. C. Hicks, D.B. Go, The impact of transition metal catalysts on macroscopic dielectric barrier discharge (DBD) characteristics in an ammonia synthesis plasma catalysis reactor, *J. Phys. Appl. Phys.* 52 (2019) 224002, <https://doi.org/10.1088/1361-6463/ab0e58>.
- [33] Y. Wang, M. Craven, X. Yu, J. Ding, P. Bryant, J. Huang, X. Tu, Plasma-enhanced catalytic synthesis of ammonia over a Ni/Al₂O₃ catalyst at Near-room temperature: insights into the importance of the catalyst Surface on the reaction mechanism, *ACS Catal.* 9 (2019) 10780–10793, <https://doi.org/10.1021/acscatal.9b02538>.
- [34] B.S. Patil, N. Cherkasov, N.V. Srinath, J. Lang, A.O. Ibadon, Q. Wang, V. Hessel, The role of heterogeneous catalysts in the plasma-catalytic ammonia synthesis, 1st Int. Conf. Nonconv. Catal. React. Appl. Catal. React. 362 (2021) 2–10, <https://doi.org/10.1016/j.cattod.2020.06.074>.
- [35] C. Ndayirinde, Y. Gorbanev, R.-G. Ciocarlan, R. De Meyer, A. Smets, E. Vlasov, S. Bals, P. Cool, A. Bogaerts, Plasma-catalytic ammonia synthesis: packed catalysts act as plasma modifiers, *Catal. Today* (2023) 114156, <https://doi.org/10.1016/j.cattod.2023.114156>.
- [36] J.A. Andersen, J.M. Christensen, M. Østberg, A. Bogaerts, A.D. Jensen, Plasma-catalytic ammonia decomposition using a packed-bed dielectric barrier discharge reactor, *Int. J. Hydrog. Energy* 47 (2022) 32081–32091, <https://doi.org/10.1016/j.ijhydene.2022.07.102>.
- [37] B.S. Patil, N. Cherkasov, J. Lang, A.O. Ibadon, V. Hessel, Q. Wang, Low temperature plasma-catalytic NO_x synthesis in a packed DBD reactor: effect of support materials and supported active metal oxides, *Appl. Catal. B Environ.* 194 (2016) 123–133, <https://doi.org/10.1016/j.apcatb.2016.04.055>.
- [38] T. Butterworth, R. Elder, R. Allen, Effects of particle size on CO₂ reduction and discharge characteristics in a packed bed plasma reactor, *Chem. Eng. J.* 293 (2016) 55–67, <https://doi.org/10.1016/j.cej.2016.02.047>.
- [39] D. Mei, X. Zhu, Y.-L. He, J.D. Yan, X. Tu, Plasma-assisted conversion of CO₂ in a dielectric barrier discharge reactor: understanding the effect of packing materials, *Plasma Sources Sci. Technol.* 24 (2014) 015011, <https://doi.org/10.1088/0963-0252/24/1/015011>.
- [40] F.J.J. Peeters, M.C.M. van de Sanden, The influence of partial surface discharging on the electrical characterization of DBDs, *Plasma Sources Sci. Technol.* 24 (2014) 015016, <https://doi.org/10.1088/0963-0252/24/1/015016>.

- [41] B. Seynnaeve, J. Lauwaert, P. Van Der Voort, A. Verberckmoes, Comprehensive model for the synthesis of γ -Al₂O₃ microsphere-supported Bimetallic iron- and copper oxide materials, *ACS Omega* 7 (2022) 41796–41803, <https://doi.org/10.1021/acsomega.2c06273>.
- [42] X. Gao, Z. Lin, T. Li, L. Huang, J. Zhang, S. Askari, N. Dewangan, A. Jangam, S. Kawi, Recent developments in dielectric Barrier Discharge plasma-assisted catalytic dry reforming of methane over Ni-based catalysts, *Catalysts* 11 (2021) 455, <https://doi.org/10.3390/catal11040455>.
- [43] K. Stanley, S. Kelly, J.A. Sullivan, Effect of ni NP morphology on catalyst performance in non-thermal plasma-assisted dry reforming of methane, *Appl. Catal. B Environ.* 328 (2023) 122533, <https://doi.org/10.1016/j.apcatb.2023.122533>.
- [44] X. Li, Y. Jiao, Y. Cui, C. Dai, P. Ren, C. Song, X. Ma, Synergistic catalysis of the synthesis of ammonia with co-based catalysts and plasma: from Nanoparticles to a single atom, *ACS Appl. Mater. Interfaces* 13 (2021) 52498–52507, <https://doi.org/10.1021/acami.1c12695>.
- [45] Y. Gorbanev, Y. Engelmann, K. van't Veer, E. Vlasov, C. Ndayirinde, Y. Yi, S. Bals, A. Bogaerts, Al₂O₃-supported transition metals for plasma-catalytic NH₃ synthesis in a DBD plasma: metal activity and insights into mechanisms, *Catalysts* 11 (2021), <https://doi.org/10.3390/catal11101230>.
- [46] Y. Uytendhouwen, V. Meynen, P. Cool, A. Bogaerts, The potential use of Core-Shell structured spheres in a packed-bed DBD plasma reactor for CO₂ conversion, *Catalysts* 10 (2020), <https://doi.org/10.3390/catal10050530>.
- [47] A. Nanakoudis, SEM: types of electrons and the information they provide, *Adv. Mater.* 2019 <https://www.thermofisher.com/blog/materials/sem-signal-types-electrons-and-the-information-they-provide/> (accessed September 22, 2023).
- [48] What does Bronkhorst mean by ln/min or ls/min?, Bronkhorst (n.d.). <https://www.bronkhorst.com/int/service-support-1/faq/flow-theory/what-does-bronkhorst-mean-by-ln-min-or-ls-min/> (accessed February 28, 2023).
- [49] N. Pinhão, A. Moura, J.B. Branco, J. Neves, Influence of gas expansion on process parameters in non-thermal plasma plug-flow reactors: a study applied to dry reforming of methane, *Int. J. Hydrog. Energy* 41 (2016) 9245–9255, <https://doi.org/10.1016/j.ijhydene.2016.04.148>.
- [50] B. Wanten, R. Vertongen, R. De Meyer, A. Bogaerts, Plasma-based CO₂ conversion: how to correctly analyze the performance? *J. Energy Chem.* (2023) <https://doi.org/10.1016/j.jechem.2023.07.005>.
- [51] Y. Uytendhouwen, K.M. Bal, I. Michielsen, E.C. Neyts, V. Meynen, P. Cool, A. Bogaerts, How process parameters and packing materials tune chemical equilibrium and kinetics in plasma-based CO₂ conversion, *Chem. Eng. J.* 372 (2019) 1253–1264, <https://doi.org/10.1016/j.cej.2019.05.008>.
- [52] F. Peeters, T. Butterworth, in: *Electrical Diagnostics of Dielectric Barrier Discharges*, Atmospheric Press, Plasma, IntechOpen, Rijeka, 2018, p. p. Ch. 2., <https://doi.org/10.5772/intechopen.80433>.
- [53] N. Jidenko, M. Petit, J.P. Borra, Electrical characterization of microdischarges produced by dielectric barrier discharge in dry air at atmospheric pressure, *J. Phys. Appl. Phys.* 39 (2006) 281–293, <https://doi.org/10.1088/0022-3727/39/2/008>.
- [54] 4100.pdf, (n.d.). <https://www.pearsonelectronics.com/pdf/4100.pdf> (accessed March 28, 2023).
- [55] M. Bueno, Weber bechelany, klotz, farrusseng, impregnation protocols on alumina beads for controlling the preparation of supported metal catalysts, *Catalysts* 9 (2019) 577, <https://doi.org/10.3390/catal9070577>.
- [56] B. Seynnaeve, J. Lauwaert, P. Vermeir, P. Van Der Voort, A. Verberckmoes, Model-based control of iron- and copper oxide particle distributions in porous γ -Al₂O₃ microspheres through careful tuning of the interactions during impregnation, *Mater. Chem. Phys.* 276 (2022) 125428, <https://doi.org/10.1016/j.matchemphys.2021.125428>.
- [57] N. Gherardi, G. Gouda, E. Gat, A. Ricard, F. Massines, Transition from glow silent discharge to micro-discharges in nitrogen gas, *Plasma Sources Sci. Technol.* 9 (2000) 340, <https://doi.org/10.1088/0963-0252/9/3/312>.
- [58] H.-H. Kim, Y. Teramoto, A. Ogata, Time-resolved imaging of positive pulsed corona-induced surface streamers on TiO₂ and γ -Al₂O₃-supported Ag catalysts, *J. Phys. Appl. Phys.* 49 (2016) 415204, <https://doi.org/10.1088/0022-3727/49/41/415204>.
- [59] S. Suzuki, H. Itoh, Gradual increase in secondary ionization coefficient γ and charge accumulation on a dielectric electrode during DBD with repeated breakdown, *Plasma Sources Sci. Technol.* 24 (2015) 055016, <https://doi.org/10.1088/0963-0252/24/5/055016>.
- [60] M.A. Cazalilla, N. Lorente, R.D. Muiño, J.-P. Gauyacq, D. Teillet-Billy, P. M. Echenique, Theory of auger neutralization and deexcitation of slow ions at metal surfaces, *Phys. Rev. B* 58 (1998) 13991–14006, <https://doi.org/10.1103/PhysRevB.58.13991>.
- [61] F. Massines, N. Gherardi, N. Naudé, P. Ségur, Recent advances in the understanding of homogeneous dielectric barrier discharges, *Eur. Phys. J. - Appl. Phys.* 47 (2009) 22805, <https://doi.org/10.1051/epjap/2009064>.
- [62] B. Bhushan, ed., *Cold Field Electron Emission from Nanostructured Materials*, in: *Encycl. Nanotechnol.*, Springer Netherlands, Dordrecht, 2016: pp. 604–604.
- [63] J. Kruszelnicki, K.W. Engeling, J.E. Foster, Z. Xiong, M.J. Kushner, Propagation of negative electrical discharges through 2-dimensional packed bed reactors, *J. Phys. Appl. Phys.* 50 (2016) 025203, <https://doi.org/10.1088/1361-6463/50/2/025203>.
- [64] W. Wang, H.-H. Kim, K. Van Laer, A. Bogaerts, Streamer propagation in a packed bed plasma reactor for plasma catalysis applications, *Chem. Eng. J.* 334 (2018) 2467–2479, <https://doi.org/10.1016/j.cej.2017.11.139>.
- [65] R. Brandenburg, Dielectric barrier discharges: progress on plasma sources and on the understanding of regimes and single filaments, *Plasma Sources Sci. Technol.* 26 (2017) 053001, <https://doi.org/10.1088/1361-6595/aa6426>.
- [66] C. Bajon, S. Dap, A. Belinger, O. Guaitella, T. Hoder, N. Naudé, Homogeneous dielectric barrier discharge in CO₂, *Plasma Sources Sci. Technol.* 32 (2023) 045012, <https://doi.org/10.1088/1361-6595/acc9d9>.
- [67] R. Snoeckx, R. Aerts, X. Tu, A. Bogaerts, Plasma-based dry reforming: a computational study ranging from the Nanoseconds to seconds time scale, *J. Phys. Chem. C* 117 (2013) 4957–4970, <https://doi.org/10.1021/jp311912b>.
- [68] J. Van Turnhout, D. Aceto, A. Travert, P. Bazin, F. Thibault-Starzyk, A. Bogaerts, F. Azzolina-Jury, Observation of surface species in plasma-catalytic dry reforming of methane in a novel atmospheric pressure dielectric barrier discharge *in situ* IR cell, *CatalSci. Technol.* 12 (2022) 6676–6686, <https://doi.org/10.1039/D2CY00311B>.
- [69] A. Parastaev, N. Kosinov, E.J.M. Hensen, Mechanistic study of catalytic CO₂ hydrogenation in a plasma by operando DRIFT spectroscopy, *J. Phys. Appl. Phys.* 54 (2021) 264004, <https://doi.org/10.1088/1361-6463/abeb96>.
- [70] E.K. Gibson, C.E. Stere, B. Curran-McAteer, W. Jones, G. Cibin, D. Gianolio, A. Goguet, P.P. Wells, C.R.A. Catlow, P. Collier, P. Hinde, C. Hardacre, Probing the role of a non-thermal plasma (NTP) in the hybrid NTP catalytic oxidation of methane, *Angew. Chem. Int. Ed.* 56 (2017) 9351–9355, <https://doi.org/10.1002/anie.201703550>.
- [71] P. Barboun, P. Mehta, F.A. Herrera, D.B. Go, W.F. Schneider, J.C. Hicks, Distinguishing plasma contributions to catalyst performance in plasma-assisted ammonia synthesis, *ACS Sustain. Chem. Eng.* 7 (2019) 8621–8630, <https://doi.org/10.1021/acssuschemeng.9b00406>.
- [72] Y. Engelmann, P. Mehta, E.C. Neyts, W.F. Schneider, A. Bogaerts, Predicted influence of plasma activation on nonoxidative coupling of methane on transition metal catalysts, *ACS Sustain. Chem. Eng.* 8 (2020) 6043–6054, <https://doi.org/10.1021/acssuschemeng.0c00906>.
- [73] L. Hollevoet, E. Vervloessem, Y. Gorbanev, A. Nikiforov, N. De Geyter, A. Bogaerts, J.A. Martens, Energy-efficient small-scale ammonia synthesis process with plasma-enabled nitrogen oxidation and catalytic reduction of adsorbed NO_x, *ChemSusChem* 15 (2022) e202102526, <https://doi.org/10.1002/cssc.202102526>.
- [74] Y. Engelmann, K. Van 't Veer, Y. Gorbanev, E.C. Neyts, W.F. Schneider, A. Bogaerts, Plasma catalysis for ammonia synthesis: a microkinetic modeling study on the contributions of eley-rideal reactions, *ACS Sustain Chem. Eng.* 9 (2021) 13151–13163, <https://doi.org/10.1021/acssuschemeng.1c02713>.